


---

This is the **accepted version** of the journal article:

Sciortino, Giuseppe; Sanna, Daniele; Ugone, Valeria; [et al.]. «Decoding Surface Interaction of VIVO Metallo-drug Candidates with Lysozyme». *Inorganic Chemistry*, Vol. 57, Issue 8 (April 2018), p. 4456-4469. DOI 10.1021/acs.inorgchem.8b00134

---

This version is available at <https://ddd.uab.cat/record/281917>

under the terms of the  <sup>IN</sup> COPYRIGHT license

# Decoding surface interaction of V<sup>IV</sup>O metallodrug candidates with lysozyme

*Giuseppe Sciortino,<sup>#,§</sup> Daniele Sanna,<sup>†</sup> Valeria Ugone,<sup>§</sup> Agustí Lledós,<sup>#</sup> Jean-Didier Maréchal,<sup>\*,#</sup>  
and Eugenio Garribba<sup>\*,§</sup>*

<sup>#</sup> Departament de Química, Universitat Autònoma de Barcelona, 08193 Cerdanyola del Vallés,  
Barcelona, Spain

<sup>§</sup> Dipartimento di Chimica e Farmacia, Università di Sassari, Via Vienna 2, I-07100 Sassari, Italy

<sup>†</sup> Istituto CNR di Chimica Biomolecolare, Trav. La Crucca 3, I-07040 Sassari, Italy

Corresponding authors. E-mail: [jeandidier.marechal@uab.cat](mailto:jeandidier.marechal@uab.cat) (J-D.M.); [garribba@uniss.it](mailto:garribba@uniss.it) (E.G.).

## Abstract

The interaction of metallodrugs with proteins influences their transport, uptake and mechanism of action. In this study, we present an integrative approach based on spectroscopic (EPR) and computational (docking) tools to elucidate the non-covalent binding modes of various  $V^{IV}O$  compounds with lysozyme, a prototypical model of protein receptor. Five  $V^{IV}O$ -flavonoid drug candidates formed by quercetin (que), morin (mor), 7,8-dihydroxyflavone (7,8-dhf), chrysin (chr) and 5-hydroxyflavone (5-hf) – effective against several osteosarcoma cell lines –, and two benchmark  $V^{IV}O$  species of acetylacetone (acac) and catechol (cat), are evaluated. The results show a gradual variation of the EPR spectra at room temperature, which is associated to the strength of the interaction between the square pyramidal complexes  $[VOL_2]$  and the surface residues of lysozyme. The qualitative strength of the interaction from EPR is:  $[VO(que)_2]^{2-} \sim [VO(mor)_2] > [VO(7,8-dhf)_2]^{2-} > [VO(chr)_2] \sim [VO(5-hf)_2] > [VO(acac)_2] \sim [VO(cat)_2]^{2-}$ . This observation is compared with protein-ligand docking calculations with GOLD software examining the GoldScore scoring function – for which hydrogen bonds and van der Waals contact terms have been optimized to account for the surface interaction. The best predicted binding modes display an energy trend in good agreement with the EPR spectroscopy. Computation indicates that the strength of the interaction can be predicted by the  $F_{max}$  value and depends on the number of OH or CO groups of the ligands that can interact with different sites on the protein surface and, more particularly, with those in the vicinity of the active site of the enzyme. The interaction strength determines the type of signal revealed (*rigid limit* or *isotropic*) in the EPR spectra. Spectroscopic and computational results also suggest that there are several sites with comparable binding energy, with the V complexes distributing among them in a bound state and in aqueous solution in an unbound state. This kind of study and analysis could be generalized to determine the non-covalent binding modes of a generic metal species with a generic protein.

## Introduction

Vanadium (V) compounds exhibit a wide variety of pharmacological properties. Some have shown activity as spermicidal, anti-HIV, antiparasitic, antiviral, antituberculosis and, particularly, as antitumor and antidiabetic agents.<sup>1</sup> Bis(maltolato)oxidovanadium(IV) (BMOV) is the benchmark compound for novel vanadium candidates with antidiabetic action,<sup>2</sup> and its derivative bis(ethylmaltolato)oxidovanadium(IV) (BEOV) reached phase IIa of the clinical trials, even if the tests have provisionally been abandoned due to a series of reasons, such the renal problems arising with several patients and the expiration of the patent.<sup>3</sup> Therefore, the discovery and design of novel  $V^{IV}O^{2+}$  derivatives is an exciting challenge in medicinal inorganic chemistry.

When dealing with a V drug candidate, information on distribution and biotransformation under physiological conditions is fundamental,<sup>4, 5, 6</sup> and considering that it can reach the target cells in the same molecular form as it is administered would be an oversimplification.<sup>4, 7</sup> In fact in the blood, depending on the thermodynamic stability of the specific V compound, ligand exchange, complexation and/or redox reactions can occur. In particular, proteins and low molecular mass bioligands can interact with the V species and partly or fully displace the organic ligands L.<sup>8, 9</sup>

The interaction with proteins *in vivo* plays a key role in vanadium compounds bioactivity, because it can influence the transport in the blood, the cell uptake and the mechanism of action.<sup>10</sup> For example, V is transported in the serum mainly by human serum transferrin (hTf) which binds  $V^{III}$ ,  $V^{IV}$  and  $V^V$  in the specific sites of iron,<sup>10</sup>  $V^V$  is reduced in the cytosol to  $V^{IV}O$  species where they bind to hemoglobin,<sup>11</sup> the inhibition of phosphatase by  $H_2V^VO_4^-$  is the basis of the V antidiabetic activity,<sup>12, 13</sup> and the binding of  $V^{IV}$  or  $V^V$  species to holo-transferrin or apo-transferrin after the closure of its conformation can promote the cellular metal uptake because the close form is recognized and internalized by the transferrin receptor (TfR) in the receptor-mediated endocytosis.<sup>8h, 9g, 9h</sup>

Unfortunately, in most of the cases the lack of knowledge on the three-dimensional interaction between V compounds and proteins limits the development of new active molecules and, as a

matter of fact, this appears to be a recurrent problem in metallodrug design projects. In general, two types of binding are expected in a (metal complex)–protein system. i) A *covalent binding*, when the protein replaces with one or more side chain residues the bidentate organic ligand L coordinated to the metal or weak ligands such as water; for example, species with composition *cis*-VOL<sub>2</sub>(Protein) are formed from *cis*-VOL<sub>2</sub>(H<sub>2</sub>O), upon the replacement of the equatorial water molecule by a His-N or Asp/Glu-COO donor.<sup>8b-i, 8k, 8m, 8o, 8n, 9a, 9b, 9d-g, 9i, 10</sup> ii) A *non-covalent binding*, when the complex VOL<sub>2</sub> interacts through secondary interactions, such as van der Waals and hydrogen contacts, with the accessible groups on the protein surface; in this context, various papers were published over the last years on the surface interaction on V compounds with proteins or DNA.<sup>14</sup>

When X-ray diffraction analysis is not available, other methods are necessary to get information on (V complexes)–protein systems. For vanadium(IV), techniques such as EPR,<sup>8a-m, 8o, 9, 15</sup> ESEEM,<sup>16</sup> ENDOR,<sup>17</sup> UV-Vis,<sup>18</sup> and CD spectroscopy,<sup>9f-h</sup> gel-electrophoresis,<sup>9g, 9h</sup> and, recently, MALDI-TOF, SAXS, size-exclusion chromatography, polarography and voltammetry,<sup>15, 19</sup> were used. However, these techniques provide limited information of the molecular nature of the interaction and they might not identify the exact region of the protein where the metal is bound, the specific residues involved in the coordination or the possible stabilization of the structure through secondary coordination sphere.

Over the last years, bridging these techniques with computation has been a bet to overcome these difficulties. Computational methods were applied to predict the nature of metallodrug–protein interaction and so get information on their biological and pharmacological role. Molecular modeling has become a major element in drug design and protein–*ligand*<sup>20</sup> dockings are used to generate fast and accurate predictions of the binding of small chemical species with biomolecules and calculate both relative affinities and geometries. Some years ago, some of us showed the potential of docking algorithms in dealing the binding of organometallic compounds to proteins when no changes of the first coordination sphere of the metal occur during binding.<sup>21</sup> Going beyond the results in the literature,<sup>22</sup> we recently generated a new series of parameters in GOLD program to

treat the *covalent binding* of transition metal complexes in general and vanadium compounds in particular with proteins.<sup>23, 24</sup>

In this work an integrative EPR and docking approach was applied to the *non-covalent interaction* between the bis-chelated V<sup>IV</sup>O complexes formed by flavonoids (indicated generally with VOL<sub>2</sub>, all with anticancer activity, in particular against several osteosarcoma cell lines<sup>25</sup>) and lysozyme (Lyz). Even if data on the binding between V species and lysozyme *in vivo* are not available, Lyz can be considered a model protein and has been frequently used to study the (metal species)–protein interaction.<sup>26</sup> Two benchmark V<sup>IV</sup>O compounds of acetylacetonate (acac) and catecholate (cat) – both of them proposed as antidiabetic and anticancer potential drugs<sup>7, 27</sup> – were also evaluated. The results indicate that with this integrative approach is possible to predict the non-covalent binding modes of V<sup>IV</sup>O complexes with proteins (both *in vitro* and *in vivo*). This approach could be generalized to the non-covalent binding modes of any V<sup>IV</sup>O complex to the proteins and, also, to the surface interaction of a generic metal species with a generic protein.

## Computational and experimental methods

**Computational section.** The geometry of all the V<sup>IV</sup>O complexes has been optimized through DFT methods with Gaussian 09 software<sup>28</sup> using the functional B3P86 and the basis set 6-311g, according to the procedure established in the literature.<sup>8j, 29</sup> This level of theory describes with high accuracy the structures of first-row metal compounds,<sup>30</sup> and in particular V complexes.<sup>29a</sup>

All docking calculations were performed with GOLD 5.2,<sup>31</sup> the most convenient software to describe our systems. The X-ray structure of lysozyme (PDB code: 2lyz<sup>32</sup>) was obtained from the Protein Data Bank.<sup>33</sup> The crystallographic water and all the other small molecules present in the structure have been removed and hydrogen atoms were added with USCF Chimera.<sup>34</sup>

The GOLD parameter file was modified to include parameters of atom types not included in GOLD's database such as V and the keto oxygen coordinated to the metal (e.g. morin). The V atom type (M.V4) was build with the values reported in the literature<sup>14b</sup> and the keto oxygen (O.pl3) was build considering the VSEPR theory, according with what was recently published.<sup>23-24</sup>

The calculations were carried out using a customized version of GoldScore scoring function (*Fitness* or *F*). This scoring function was selected since it was found in our recent study to be the most tunable scoring function of the GOLD suite.<sup>24</sup> It is represented in eq. (1).

$$Fitness (F) = \alpha \cdot S_{hbond}^{ext} + \beta \cdot S_{vdW}^{ext} + \gamma \cdot S_{hbond}^{int} + \delta \cdot (S_{vdW}^{int} - S_{tors}) \quad (1)$$

where  $S_{hbond}^{ext}$  and  $S_{vdW}^{ext}$  are the scoring terms related to the hydrogen (*hbond*) and van der Waals (*vdW*) intermolecular interactions.  $S_{hbond}^{int}$  represents the intramolecular *hbond* interactions and  $S_{tors}$  evaluates the change in stability due to the molecular torsions.  $\alpha$ ,  $\beta$ ,  $\gamma$ , and  $\delta$  are empirical coefficients optimized to weigh the different interactions. To reproduce the experimental results of the examined systems the weight of the term  $S_{vdW}^{ext}$ , related to the *vdW* intermolecular interaction, has been changed and set to 0.3 (instead of the default value of 1.375). The other parameters ( $\alpha$ ,  $\gamma$ , and  $\delta$ ) were set to 1.0. This combination of  $\alpha$ ,  $\beta$ ,  $\gamma$ , and  $\delta$  values ensures, for our systems, a very good balance between the relative weight of the *hbond* and *vdW* interactions for this type of systems.

In all the calculations the spatial coordinates of the complexes have been randomized before the simulations. Genetic algorithm (GA) parameters have been set to 100 GA runs with a minimum of 100,000 operations. The rest of the parameters, including pressure, number of islands, niche size, crossover, mutation and migration were set to default. The evaluation space was built to contain all the protein with a sphere with radius equal to 28 Å. Finally, the docking solutions were analysed by

means of GaudiView, an *in-house* graphical interface developed as an extension for Chimera software.<sup>35</sup>

The best solutions of the calculations were evaluated through two main criteria: (i) the scoring function (*Fitness*) associated with each pose, as reported in eq. (1) and (ii) the population of the clusters containing the best structure. The term cluster refers to any set of solutions or poses which obtain a root mean square deviation (RMSD) less or equal than a selected cut-off, while population indicates the number of solutions or poses in the identified cluster.

**Chemicals.** Water was deionized prior to use through the purification system Millipore MilliQ Academic.  $V^{IV}O^{2+}$  solutions were prepared from  $VOSO_4 \cdot 3H_2O$ .<sup>36</sup> Hen egg white lysozyme (Lyz) was purchased from Sigma with a molecular mass of 14.3 kDa. Other chemical, i.e. acetylacetone (acac), catechol (cat), quercetin (que), morin (mor), 7,8-dihydroxyflavone (7,8-dhf), 5-hydroxyflavone (5-hf), chrysin (chr), and 4-(2-hydroxyethyl)piperazine-1-ethanesulfonic acid (HEPES) were Aldrich products of the highest grade available and used as received.

**Preparation of the solutions and EPR measurements.** All the solutions were freshly prepared by weighing all the components before each experiment. In particular, these were prepared dissolving in ultra-pure water  $VOSO_4 \cdot 3H_2O$  to obtain a  $V^{IV}O^{2+}$  concentration of  $(0.5-1.0) \times 10^{-3}$  M. Argon was bubbled through the solutions to ensure the absence of oxygen and, under these conditions, the oxidation of  $V^{IV}$  to  $V^V$  is negligible. To the solution containing the metal ion, the ligand L (acac, cat, que, mor, 7,8-dhf, 5-hf, chr) was added to reach a metal to ligand ratio of 1:2. HEPES ( $1.0 \times 10^{-1}$  M) was used as buffer and does not bind the metal species nor interfere with the experiments. Subsequently, pH was raised to *ca.* 7.4 and to 1 mL of this solution, again carefully purged with argon, Lyz was added to obtain a concentration of  $7.0 \times 10^{-4}$  M. The model systems  $V^{IV}O^{2+}/L$  were previously examined in the literature.<sup>8k,37</sup>

EPR spectra were recorded from 2000 to 5000 Gauss at liquid nitrogen temperature (LNT, 77 K) or room temperature (RT, 298 K) with an X-band Bruker EMX spectrometer equipped with a HP 53150A microwave frequency counter. The microwave frequency was in the range 9.40-9.41 GHz



for the LNT spectra, and in the range 9.83-9.85 GHz for those at RT. Microwave power was 20 mW (which is, with the ER4119 HS resonator, below the saturation limit), time constant was 81.92 ms, modulation frequency 100 kHz, modulation amplitude 0.4 mT, resolution 4096 points. To extract the experimental spin Hamiltonian parameters, the spectra were generated with WinEPR SimFonia software.<sup>38</sup>

**Background theory of EPR spectroscopy.**  $V^{IV}O^{2+}$  ion has a  $d^1$  electronic configuration with one unpaired electron. The isotropic ( $A_{iso}$ ) or anisotropic ( $A_x, A_y, A_z$ ) hyperfine coupling constants in an EPR spectrum arise from the interaction between the spin angular momentum of the electron ( $S = 1/2$ ) with the spin angular momentum of  $^{51}V$  nucleus ( $I = 7/2$ , 99.8% natural abundance). Among the three anisotropic constant,  $A_z$  is more sensitive to the equatorial donors than  $A_x$  and  $A_y$ . The value of  $A_{iso}$  and  $A_z$  depends on the electron donor capacity of the ligands, with the most donating ligands contributing the least to the coupling constant, as suggested by the “additivity relationship”.<sup>39, 40, 41</sup>

For all the complexes a *rigid limit* EPR spectrum is predicted in frozen solutions (for example, at LNT) because the molecules are blocked in their positions. When the spectra are recorded on a liquid solution at RT, for small complexes  $VOL_2$  formed by a low molecular mass ligand L, an *isotropic* spectrum is expected because the rotational motion of the chemical species is faster than the timescale of EPR spectroscopy ( $\sim 50$  ns<sup>42</sup>), whereas for large complexes, such as the ternary  $V^{IV}O-L-Protein$ , a *slow tumbling* type spectrum is expected because the rotational motion of the species is slowed down.<sup>8f</sup> The slower the rotational motion, the more the spectrum approaches to the *rigid limit* type.<sup>43</sup>

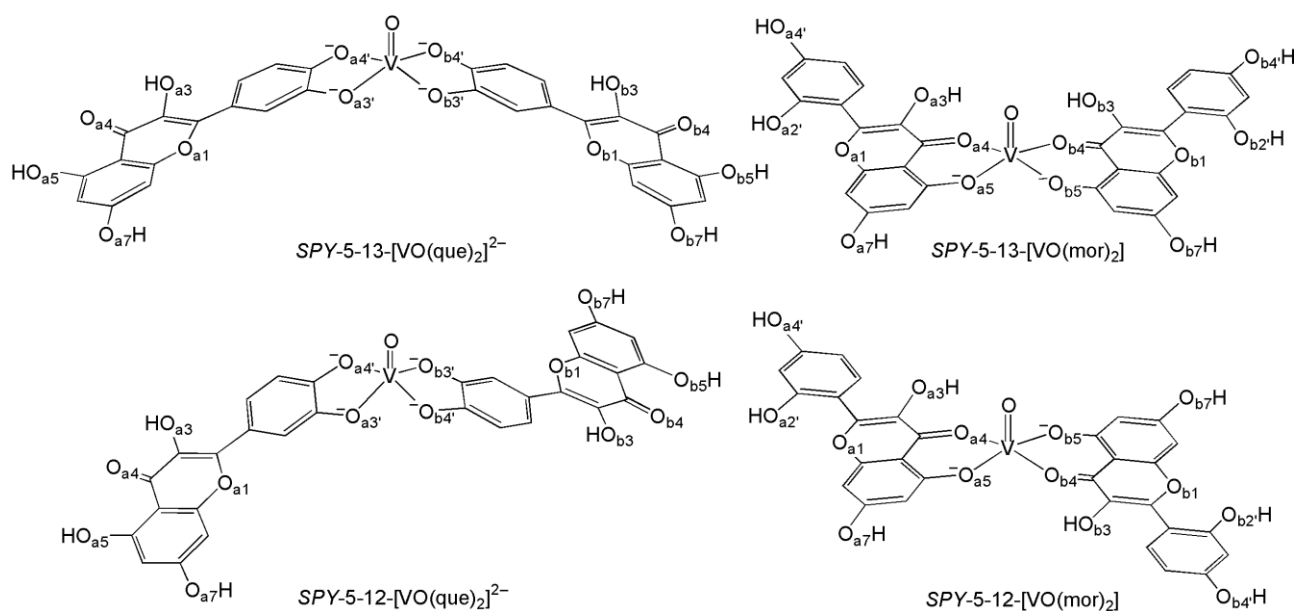
For the systems examined in this study, two types of interactions are, in principle, possible.

i) *Covalent binding* of lysozyme to V through one or more donors of the protein residues. In this case a *rigid limit* EPR spectrum is expected at RT and a change of the  $^{51}V$   $A_z$  value of the ternary  $V^{IV}O-L-Lyz$  species will be observed due to the different equatorial donor set with respect to  $VOL_2$ .

ii) *Non-covalent binding* of VOL<sub>2</sub> to lysozyme which, at RT, can result in a *rigid limit* spectrum if the interaction is so strong that the most of species are blocked on the protein surface or – in contrast – a *slow tumbling* or an *isotropic* spectrum if the interaction is weak and most of the complexes is free in solution. In the first case, the value of  $A$  measured at RT will be comparable with  $A_z$  measured at LNT for VOL<sub>2</sub> (indeed, in both the cases the species is blocked, by interaction with the protein at RT or upon freezing at LNT); in the second case the value of  $A$  will be close to  $A_{iso}$  if the spectrum is completely *isotropic* or of the *slow tumbling* type.

## Results and discussion

(1). Systems V<sup>IV</sup>O<sup>2+</sup>/que/Lyz and V<sup>IV</sup>O<sup>2+</sup>/mor/Lyz. Spectroscopic and computational data indicate that, under physiological pH, quercetin and morin form square pyramidal V<sup>IV</sup>O species with composition [VO(que)<sub>2</sub>]<sup>2-</sup> and [VO(mor)<sub>2</sub>], binding V with (O<sup>-</sup>, O<sup>-</sup>) and (CO, O<sup>-</sup>) donor set, respectively, similar to those of catecholate and acetylacetonate (Scheme 1).<sup>37</sup> For penta-coordinated complexes, in principle, two different structures are possible, depending on the position of the O donors (*trans* or *cis*, see Scheme 1). According to IUPAC nomenclature, they are named SPY-5-12 and SPY-5-13.<sup>44</sup>



**Scheme 1.** Possible isomers of  $[\text{VO}(\text{que})_2]^{2-}$  and  $[\text{VO}(\text{mor})_2]$  species formed by quercetinate(2-) and morinate(-) anions. With the numbers the position of O atoms on the three rings is indicated, while with the subscripts a and b the two different ligands are denoted.

EPR spectra recorded in the system containing  $\text{V}^{\text{IV}}\text{O}^{2+}$ , que or mor and lysozyme are shown in **Figure 1** (que) and **Figure S1** (mor) of Supporting Information. At 298 K (RT) the spectra recorded at pH 7.4 in the binary systems  $\text{V}^{\text{IV}}\text{O}^{2+}/\text{que}$  and  $\text{V}^{\text{IV}}\text{O}^{2+}/\text{mor}$  are of the *slow tumbling* type, while – in contrast – those measured in the ternary system with lysozyme are significantly different and can be classified as *rigid limit* (trace b of **Figures 1 and S1**), indicating that the rotational motion of the complexes  $[\text{VO}(\text{que})_2]^{2-}$  and  $[\text{VO}(\text{mor})_2]$  is prevented by the interaction with the protein. As it is possible to observe, the pattern and the spin Hamiltonian parameters extracted in the ternary systems ( $g_z = 1.954$ ,  $A_z = 152.4 \times 10^{-4} \text{ cm}^{-1}$  for  $\text{V}^{\text{IV}}\text{O}^{2+}/\text{que}/\text{Lyz}$ , and  $g_z = 1.950$ ,  $A_z = 163.3 \times 10^{-4} \text{ cm}^{-1}$  for  $\text{V}^{\text{IV}}\text{O}^{2+}/\text{mor}/\text{Lyz}$ ) are comparable to those obtained at 77 K (LNT) for the bis-chelated complexes  $[\text{VO}(\text{que})_2]^{2-}$  ( $g_z = 1.955$ ,  $A_z = 155.7 \times 10^{-4} \text{ cm}^{-1}$  <sup>37</sup>) and  $[\text{VO}(\text{mor})_2]$  ( $g_z = 1.952$ ,  $A_z = 164.4 \times 10^{-4} \text{ cm}^{-1}$  <sup>37</sup>). The slight increase of  $A_z$  for  $[\text{VO}(\text{que})_2]^{2-}$  and  $[\text{VO}(\text{mor})_2]$  from LNT to RT (cfr. traces a and b of **Figure 1** and **Figure S1**) is due to the influence of the stress associated with ice crystal formation, as already discussed for the interaction of  $\text{Cu}^{\text{II}}$  with proteins.<sup>45</sup>

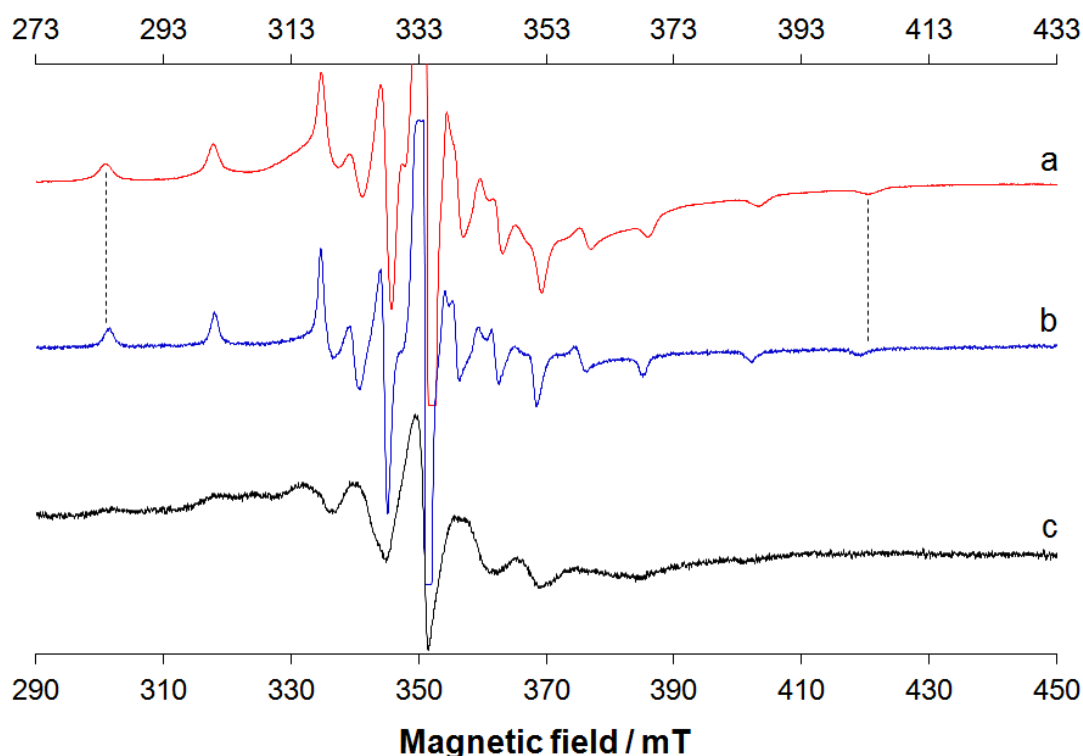


**Figure 1.** X-band EPR spectra recorded at pH 7.40 on: a) binary system  $V^{IV}O^{2+}/\text{que}$  1/2 at 77 K and  $\nu = 9.406$  GHz ( $V^{IV}O^{2+}$  concentration  $1.0 \times 10^{-3}$  M); b) ternary system  $V^{IV}O^{2+}/\text{que}/\text{Lyz}$  1/2/1 at 298 K and  $\nu = 9.852$  GHz ( $V^{IV}O^{2+}$  concentration  $7.0 \times 10^{-4}$  M) and c) binary system  $V^{IV}O^{2+}/\text{que}$  1/2 at 298 K and  $\nu = 9.852$  GHz ( $V^{IV}O^{2+}$  concentration  $7.0 \times 10^{-4}$  M). The magnetic field in the upper axis refers to the trace a, and that in the lower axis to the traces b and c. With the dotted line the position of the  $M_1 = -7/2, 7/2$  resonances of  $[\text{VO}(\text{que})_2]^{2-}$  at 77 K are indicated.

It must be observed that: i) in the binary and ternary systems with Lyz the same species exist in aqueous solution and, from the comparison of spectra, these are  $[\text{VO}(\text{que})_2]^{2-}$  and  $[\text{VO}(\text{mor})_2]$ , respectively; ii) at RT in the systems  $V^{IV}O^{2+}/\text{que}/\text{Lyz}$  and  $V^{IV}O^{2+}/\text{mor}/\text{Lyz}$ , even if lysozyme does not directly interact with vanadium through a *covalent bond*, the EPR signals of  $[\text{VO}(\text{que})_2]^{2-}$  and  $[\text{VO}(\text{mor})_2]$  are *rigid limit*, while one should expect an *isotropic* or a *slow tumbling* spectrum for these low molecular mass species (see Background theory of EPR spectroscopy section in the

Computational and Experimental Methods). This apparent inconsistency can be explained supposing that que and mor anions coordinated to  $V^{IV}O^{2+}$  interact with lysozyme, blocking the fast tumbling in solution. As indicated by EPR spectroscopy, such an interaction should involve only *hbond* and *vdW* contacts and not *covalent bonds* between  $[VO(que)_2]^{2-}$  or  $[VO(mor)_2]$  and surface residues of lysozyme. As a first hypothesis, this can be explained through the formation of a network of hydrogen bonds through the  $O^-$ , OH and CO groups of quercetin and morin with the polar side chains of the protein.

To study the nature of the interaction between the two isomers *SPY-5-12* and *SPY-5-13* of  $[VO(que)_2]^{2-}$  and  $[VO(mor)_2]$  and lysozyme, docking calculations were carried out. The geometry of the two isomers was optimised with DFT methods and, subsequently, blind docking calculations were performed using the structure of lysozyme available in PDB (2lyz [32](#)). The results are listed in **Table 1** (que) and **Table S1 of Supporting Information** (mor).

**Table 1.** Docking results of the interaction of  $[VO(que)_2]^{2-}$  with lysozyme.

Cluster <sup>a</sup>	Interacting residue	Distance O...X <sup>b</sup>	$F_{max}$ <sup>c</sup>	$F_{mean}$ <sup>d</sup>	Pop. <sup>e</sup>
<b><i>SPY-5-13</i></b> <sup>f</sup>					
I cluster	HO <sub>a7</sub> ...Arg61(NH <sub>2</sub> )	2.474	21.95	21.26	7/100
	HO <sub>b7</sub> ...Trp63(NH)	1.701			
	HO <sub>a3</sub> ...Asp52(COO)	2.094			
II cluster	O <sub>b7</sub> ...Lys116(NH <sub>3</sub> )	2.275	20.41	19.92	5/100
	HO <sub>a3</sub> ...Trp63(NH)	1.551			
	O <sub>a4</sub> ...Asn59(NH)	2.046			
	HO <sub>a5</sub> ...Gln57(CO)	1.448			
III cluster	HO <sub>a3</sub> ...Trp62(NH)	2.328	20.22	19.12	10/100
	VO <sub>1</sub> ...Asn103(NH <sub>2</sub> )	3.367			
	O <sub>a4</sub> ...Ser50(OH)	4.269			
	HO <sub>b7</sub> ...Asp101(COO)	2.823			

	HO <sub>a7</sub> ····Gln57(CO)	2.260			
	HO <sub>a5</sub> ····Asp52(NH)	1.771			
IV cluster	HO <sub>b7</sub> ····Asp52(COO)	1.563			
	HO <sub>b5</sub> ····Gln57(CO)	1.940	20.10	20.01	1/100
	HO <sub>b3</sub> ····Trp63(NH)	1.885			
	O <sub>b4</sub> ····Asn59(NH <sub>2</sub> )	3.358			
V cluster	HO <sub>a7</sub> ····Trp63(NH)	2.046	19.96	19.19	21/100
	O <sub>a5</sub> ····Asn37(CO)	1.449			
VI cluster	HO <sub>a5</sub> ····Asp52(COO)	2.007			
	HO <sub>a7</sub> ····Gln57(CO)	1.648	19.80	18.61	3/100
	O <sub>a4</sub> ····Ser50(OH)	4.509			
	HO <sub>a3</sub> ····Trp62(NH)	1.949			
VII cluster	HO <sub>a5</sub> ····Asp52(COO)	1.810			
	HO <sub>a7</sub> ····Gln57(CO)	2.306			
	HO <sub>a4</sub> ····Ser50(OH)	4.140	19.65	18.68	5/100
	HO <sub>a3</sub> ····Trp62(NH)	2.417			
	VO <sub>1</sub> ····Asn103(NH <sub>2</sub> )	3.619			
	HO <sub>b7</sub> ····Asp101(COO)	2.700			
VIII cluster	HO <sub>a7</sub> ····Trp62(NH)	1.862			
	HO <sub>a5</sub> ····Trp63(NH)	2.256	19.62	18.13	8/100
	HO <sub>a3</sub> ····Ala107(CO)	1.679			
<b><i>SPY-5-12</i><sup>f</sup></b>					
I cluster	HO <sub>a7</sub> ····Trp62(NH)	1.627			
	HO <sub>a5</sub> ····Trp63(NH)	2.318	19.47	18.96	63/100
	HO <sub>a3</sub> ····Ala107(CO)	1.656			
II cluster	HO <sub>b3</sub> ····Trp62(NH)	2.269			
	O <sub>b4</sub> ····Ser50(OH)	4.162	18.91	–	1/100
	HO <sub>b5</sub> ····Asp52(COO)	1.765			
	VO <sub>1</sub> ····Asn103(NH <sub>2</sub> )	2.615			

	HO <sub>b7</sub> ···Gln57(CO)	2.119			
	HO <sub>b4</sub> ···Asp52(COO)	1.651			
III cluster	HO <sub>b7</sub> ···Gln57(CO)	2.127	18.30	17.63	8/100
	HO <sub>a3</sub> ···Arg57(NH <sub>2</sub> )	2.153			
	O <sub>a4</sub> ···Arg57(NH <sub>2</sub> )	2.904			

<sup>a</sup> In the table only the clusters with the highest *Fitness* value are reported. <sup>b</sup> Distance in Å. <sup>c</sup> *Fitness* value for the most stable pose of each cluster ( $F_{\max}$ ). <sup>d</sup> Mean *Fitness* value of the GoldScore scoring function for each cluster ( $F_{\text{mean}}$ ). <sup>e</sup> Number of solutions in the identified cluster. <sup>f</sup> Isomer structure calculated with Gaussian 09 at the level of theory B3P86/6-311g.

Considering the *Fitness* values of the scoring function ( $F_{\max}$  or  $F_{\text{mean}}$  in **Tables 1 and S1 of Supporting Information**, related to the interaction energy, see eq. (1)) and the population of the clusters, it can be observed that several potential binding sites are present (shown in Figures 2 and S2) and that the docking results indicate the absence of specificity for this type of surface interaction. In other words, it is plausible to think that the square pyramidal  $[\text{VO}(\text{que})_2]^{2-}$  and  $[\text{VO}(\text{mor})_2]$  distribute between all the available sites **(remaining bound to each of them longer than the timescale of EPR spectroscopy to account for the rigid limit signal)** without a specific preference for none of them.

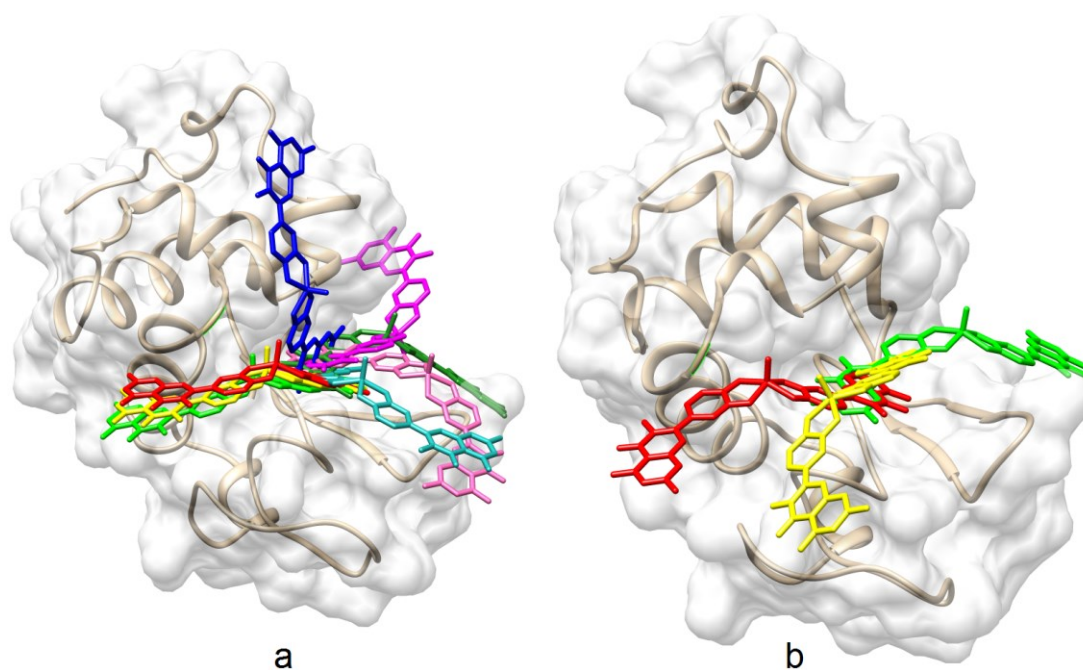


**Figure 2.** Cluster distribution for the interaction of lysozyme with the complexes *SPY*-5-13- $[\text{VO}(\text{que})_2]^{2-}$  (a), and *SPY*-5-12- $[\text{VO}(\text{que})_2]^{2-}$  (b). The eight clusters for *SPY*-5-13 and the three clusters for *SPY*-5-12 isomer are represented with different colors.

It should be noted that most of the clusters are close to the active site of the lysozyme (highlighted with a gray sphere in **Figure 3**), i.e. the large cleft to which the bacterial carbohydrate chain binds and where the cleavage of peptidoglycan cell wall occurs with the subsequent death of the bacterium.<sup>46, 47, 48</sup> On the basis of the docking results, all the residues involved in the interactions are polar and, in particular, they could be arginine (Arg12, Arg57, Arg61, Arg73, Arg112, Arg114), asparagine (Asn46, Asn59, Asn103), aspartate (Asp52, Asp101), glutamate (Glu35), tryptophan (Trp62, Trp63) or serine (Ser50). Interactions with the backbone of protein are also possible. **Figures 4 and S3** of Supporting Information illustrate the pose with highest Fitness ( $F_{\text{max}}$ ) for the interaction of the isomers *SPY*-5-13 and *SPY*-5-12 of  $[\text{VO}(\text{que})_2]^{2-}$  and  $[\text{VO}(\text{mor})_2]$  with lysozyme.

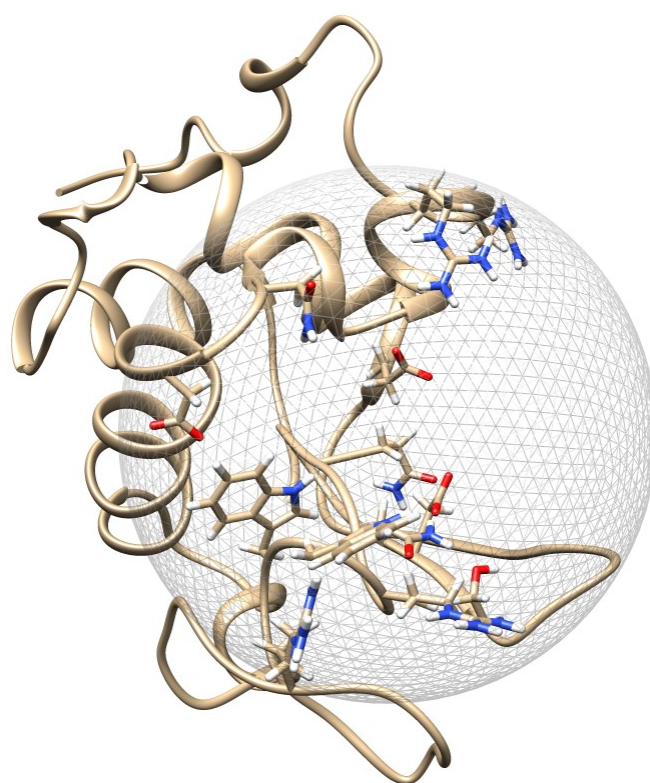




**Figure 3.** Region of lysozyme where the interaction with  $V^{IV}O$  complexes is the most probable (highlighted with a gray sphere) and residues involved in the stabilization of the poses.

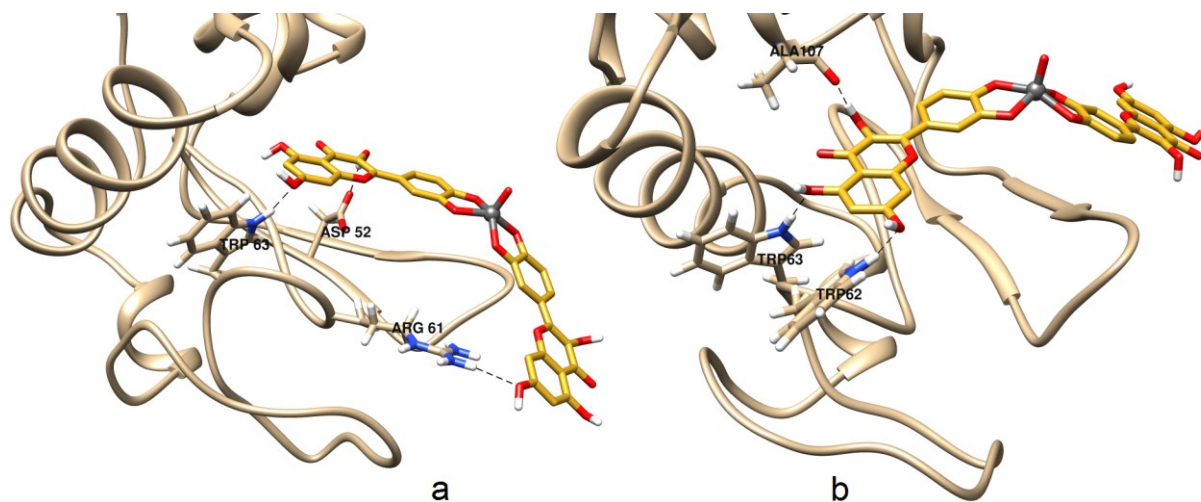
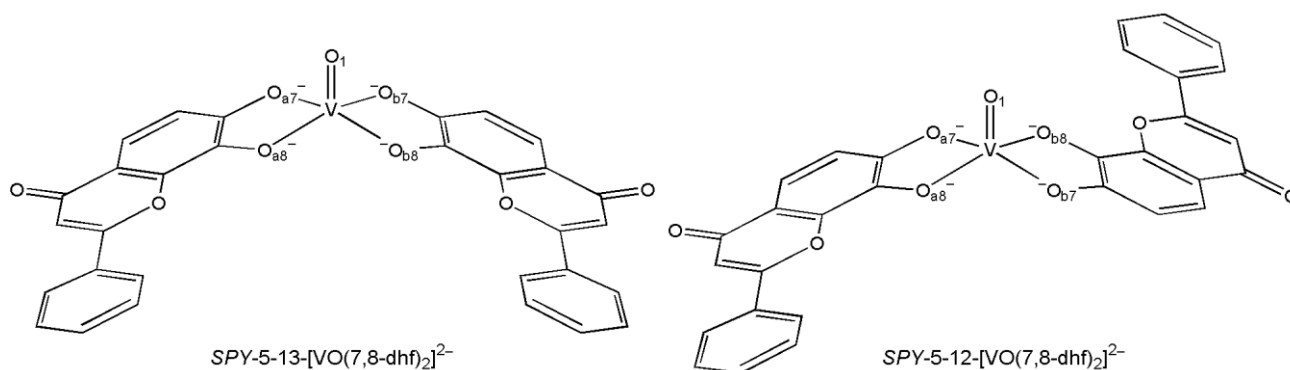


**Figure 4.** The most stable pose predicted by GOLD 5.2 for the adducts formed by  $[VO(que)_2]^{2-}$  with lysozyme: a) isomer *SPY-5-13* and b) isomer *SPY-5-12*.

(2). System  $V^{IV}O^{2+}/7,8\text{-dhf}/Lyz$ . Similarly to quercetin, 7,8-dihydroxyflavone forms at pH 7.4 a square-pyramidal  $V^{IV}O$  complex,  $[VO(7,8\text{-dhf})_2]^{2-}$ , with catecholate-like ( $O^-$ ,  $O^-$ ) coordination,<sup>37</sup> EPR spectrum is shown in the trace a of **Figure 5**, and the structure of the two possible isomers, *SPY-5-13* and *SPY-5-12* in **Scheme 2**.<sup>37</sup> EPR spin Hamiltonian parameters measured at LNT are  $g_z = 1.954$ ,  $A_z = 156.5 \times 10^{-4}$ <sup>37</sup>, very similar to those of  $[VO(que)_2]^{2-}$ , while at RT a *slow tumbling* spectrum is revealed (trace c of **Figure 5**).



**Scheme 2.** Possible isomers of  $[\text{VO}(7,8\text{-dhf})_2]^{2-}$  species formed by 7,8-dihydroxyflavonate(2-) anion. With the numbers the position of O atoms on rings A and C is indicated, while with the subscripts a and b the two different ligands are denoted.

The system  $\text{V}^{\text{IV}}\text{O}^{2+}/7,8\text{-dhf}/\text{Lyz}$  behaves in a similar but not coincident way with respect to those discussed above with quercetin and morin. Indeed, overall the EPR signals are *rigid limit* (trace b of **Figure 5**), suggesting that the interaction with the surface residues of lysozyme is strong, but *isotropic* resonances can be also revealed (indicated with the asterisks in **Figure 5**). This means that  $[\text{VO}(7,8\text{-dhf})_2]^{2-}$  distribute between the sites on the protein surface, giving a *rigid limit* EPR signal, and in aqueous solution, giving a *slow tumbling* spectrum (whose  $M_I = -7/2, 7/2$  resonances are indicated with an asterisk in **Figure 5**). In other words, the interaction between  $[\text{VO}(7,8\text{-dhf})_2]^{2-}$  and lysozyme is less strong than with  $[\text{VO}(\text{que})_2]^{2-}$  and  $[\text{VO}(\text{mor})_2]$  and a fraction of it remains free in solution.

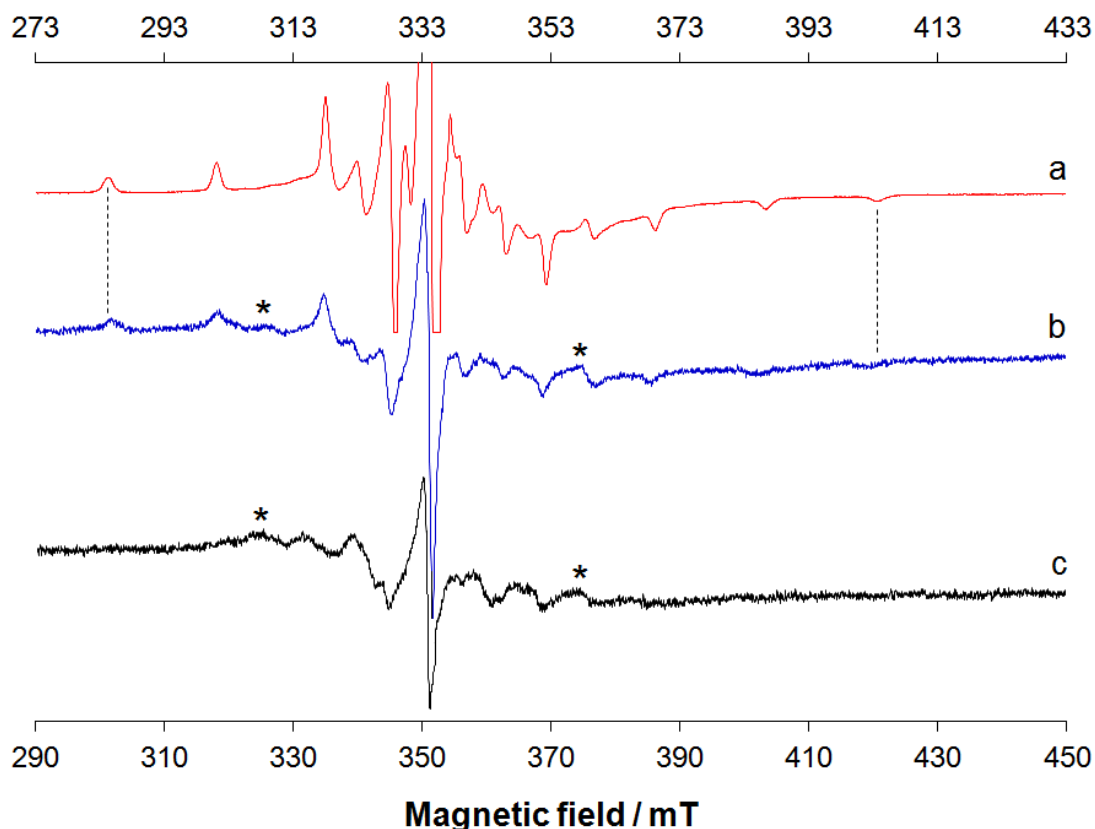


**Figure 5.** X-band EPR spectra recorded at pH 7.40 on: a) binary system  $V^{IV}O^{2+}/7,8\text{-dhf}$  1/2 at 77 K and  $\nu = 9.404$  GHz ( $V^{IV}O^{2+}$  concentration  $5.0 \times 10^{-4}$  M); b) ternary system  $V^{IV}O^{2+}/7,8\text{-dhf}/Lyz$  1/2/1 at 298 K and  $\nu = 9.834$  GHz ( $V^{IV}O^{2+}$  concentration  $7.0 \times 10^{-4}$  M) and c) binary system  $V^{IV}O^{2+}/7,8\text{-dhf}$  1/2 at 298 K and  $\nu = 9.834$  GHz ( $V^{IV}O^{2+}$  concentration  $7.0 \times 10^{-4}$  M). The magnetic field in the upper axis refers to the trace a, and that in the lower axis to the traces b and c. With the dotted line the position of the  $M_I = -7/2, 7/2$  resonances of  $[VO(7,8\text{-dhf})_2]^{2-}$  at 77 K are indicated, while with the asterisks the isotropic signals at 298 K are shown.

Docking calculations indicate that, coherently with the EPR spectra, the scoring values  $F_{\max}$  (17.16 for *SPY-5-13* and 16.97 for *SPY-5-12*, **Table 2**) are lower than those of the  $V^{IV}O$  complexes formed by quercetinate and morinate due to the minor number of *hbond* donor/acceptor groups (excluding the four coordinated O donors, only another O is present in the molecule, while que and mor have four O atoms). The solutions predicted by GOLD 5.2 are grouped, for both the isomers, mainly in one big cluster (I cluster in **Table 2**) and are situated close to the active site. The most

probable candidates for the interaction are the polar residues of arginine (Arg112) or tryptophan (Trp63). **Figure 6** illustrates the poses with highest *Fitness* and population for the interaction of [VO(7,8-dhf)<sub>2</sub>]<sup>2-</sup> with lysozyme.

**Table 2.** Docking results of the interaction of [VO(7,8-dhf)<sub>2</sub>]<sup>2-</sup> with lysozyme.

Cluster <sup>a</sup>	Interacting residue	Distance O...X <sup>b</sup>	<i>F</i> <sub>max</sub> <sup>c</sup>	<i>F</i> <sub>mean</sub> <sup>d</sup>	Pop. <sup>e</sup>
<b><i>SPY-5-13</i></b> <sup>f</sup>					
I cluster	VO <sub>1</sub> ...Arg112(NH <sub>2</sub> )	2.050	17.16	16.49	93/100
	O <sub>a</sub> ...Trp63(NH)	2.113			
II cluster	VO <sub>1</sub> ...Arg112(NH <sub>2</sub> )	2.160	16.41	–	1/100
III cluster	VO <sub>1</sub> ...Arg112(NH <sub>2</sub> )	2.017	15.01	14.98	2/100
	O <sub>b</sub> ...Trp63(NH)	1.471			
IV cluster	VO <sub>1</sub> ...Arg112(NH <sub>2</sub> )	2.081	14.76	14.68	2/100
<b><i>SPY-5-12</i></b> <sup>f</sup>					
I cluster	O <sub>b</sub> ...Trp63(NH)	2.014	16.97	16.34	98/100
	VO <sub>1</sub> ...Arg112(NH <sub>2</sub> )	2.099			
II cluster	O <sub>b</sub> ...Trp63(NH)	1.926	13.94	–	1/100
III cluster	O <sub>b</sub> ...Trp63(NH)	1.954	13.76	–	1/100

<sup>a</sup> In the table only the clusters with the highest *Fitness* value are reported. <sup>b</sup> Distance in Å. <sup>c</sup> *Fitness* value for the most stable pose of each cluster (*F*<sub>max</sub>). <sup>d</sup> Mean *Fitness* value of the GoldScore scoring function for each cluster (*F*<sub>mean</sub>). <sup>e</sup> Number of solutions in the identified cluster. <sup>f</sup> Isomer structure calculated with Gaussian 09 at the level of theory B3P86/6-311g.

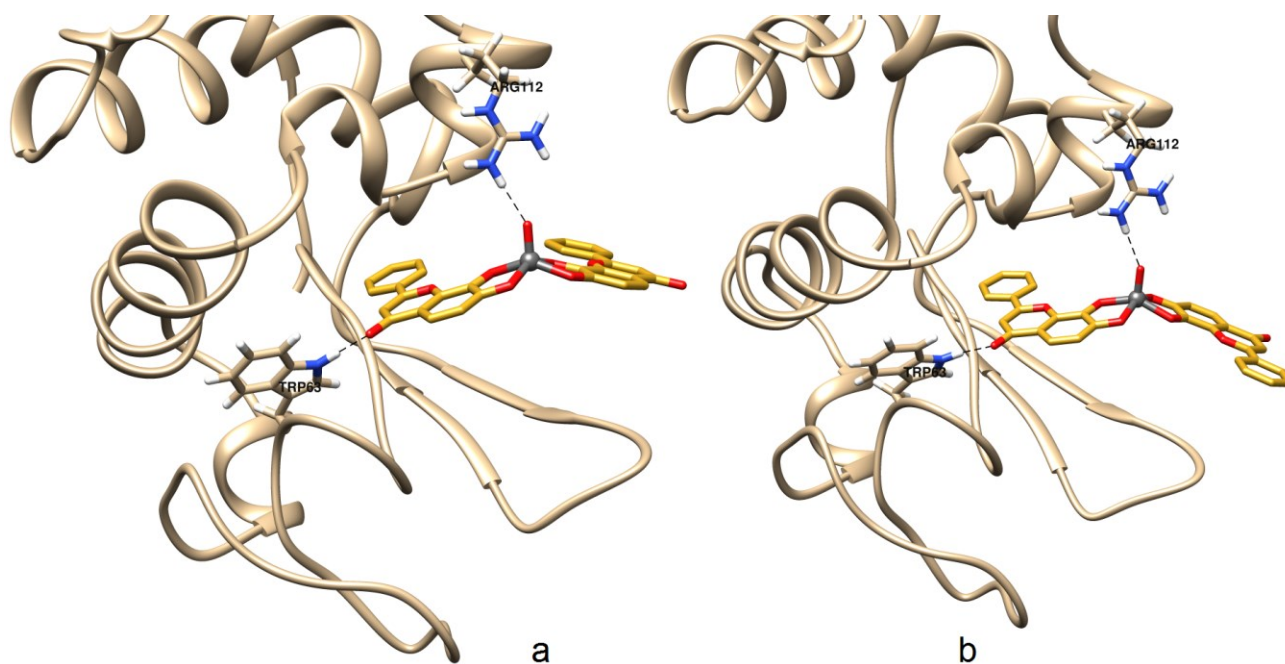
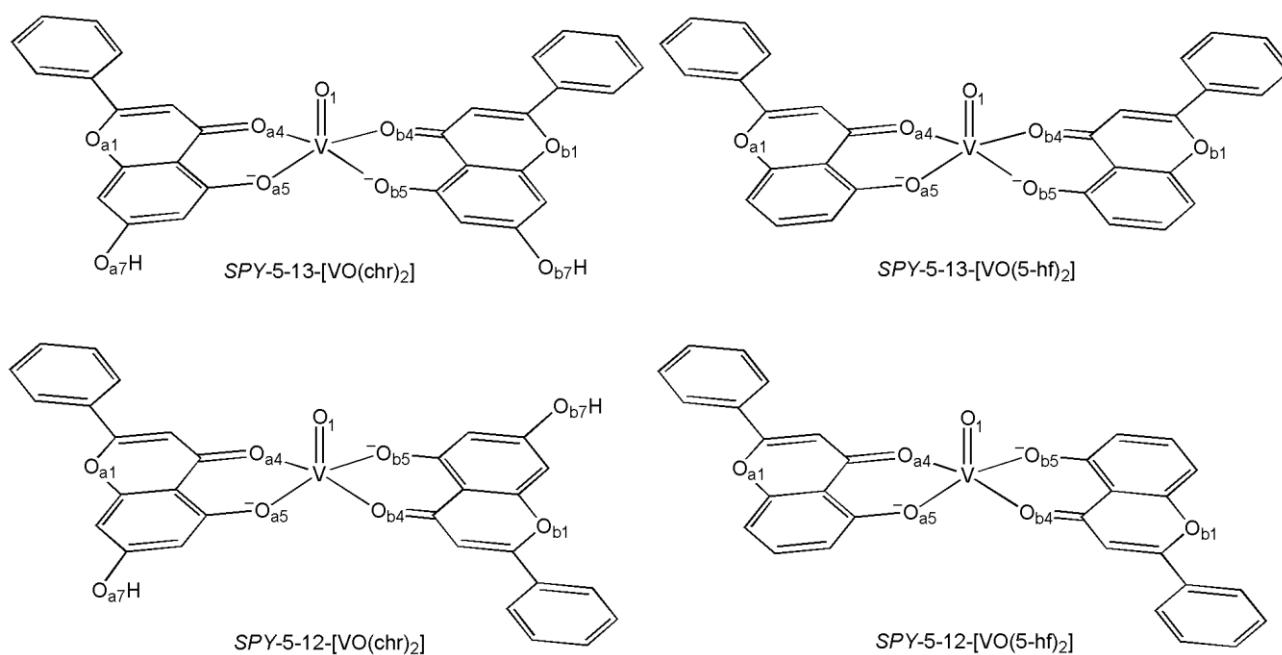


**Figure 6.** The most stable pose predicted by GOLD 5.2 for the adducts formed by  $[\text{VO}(7,8\text{-dhf})_2]^{2-}$  with lysozyme: a) isomer *SPY-5-13* and b) isomer *SPY-5-12*.

The cluster distribution for the two possible isomers of  $[\text{VO}(7,8\text{-dhf})_2]^{2-}$  is represented in **Figure S4 of Supporting Information**. In this case it can be observed that the docking calculations predict the same binding site for *SPY-5-13* and *SPY-5-12* and the only difference is the relative orientation of the V species with respect to the protein. Chemical considerations suggest that, as pointed out for  $\text{V}^{\text{IV}}\text{O}$  complexes for que and mor,  $[\text{VO}(7,8\text{-dhf})_2]^{2-}$  is not blocked indefinitely on these surface sites but that, with elapsing time, it passes from bound unbound states in the cleft of lysozyme polypeptide chain.

**(3). Systems  $\text{V}^{\text{IV}}\text{O}^{2+}/\text{chr}/\text{Lyz}$  and  $\text{V}^{\text{IV}}\text{O}^{2+}/5\text{-hf}/\text{Lyz}$ .** Chrisin and 5-hydroxyflavone form with  $\text{V}^{\text{IV}}\text{O}^{2+}$  ion at pH 7.4 square pyramidal species with the coordination of a keto-O and phenolate-O<sup>-</sup>.<sup>37</sup> The structures of the possible isomers *SPY-5-12* and *SPY-5-13* are shown in **Scheme 3**.



**Scheme 3.** Possible isomers of  $[\text{VO}(\text{chr})_2]$  and of  $[\text{VO}(5\text{-hf})_2]$  species formed by chrysinate(–) and 5-hydroxyflavonate(–) anions. With the numbers the position of O atoms on the rings A and C is indicated, while with the subscripts a and b the two different ligands are denoted.

EPR spectra measured at RT in the systems with  $\text{V}^{\text{IV}}\text{O}^{2+}$ , chrisin and lysozyme are reported in **Figure S5 of Supporting Information**. It can be noticed that the behavior changes completely with respect to the systems with quercetin, morin and 7,8-dihydroxyflavone. In particular, the spectrum recorded in the ternary system belongs to the *slow tumbling* type and is perfectly coincident with that of the binary system (cfr. traces a and b of **Figure S5**). **This means that the interaction between  $[\text{VO}(\text{chr})_2]$  and Lyz is weaker than those revealed for the previous complexes and, in the EPR timescale, the bis-chelated V complex is present in aqueous solution and its rotational motion is not blocked nor slowed down.**

The results of the docking calculations for the interaction of the isomers *SPY-5-13* and *SPY-5-12* of  $[\text{VO}(\text{chr})_2]$  with lysozyme are reported in **Table S2**, while **Figure S6** shows the most stable poses. It can be observed that the residues involved in the *hbond* and *vdW* contacts are arginine (Arg73, Arg112), glutamate (Glu35), aspartate (Asp52, Asp101), asparagine (Asn59, Asn103), threonine

(Thr47), and tryptophan (Trp62, Trp63). The bond V=O points toward the protein, whereas for  $[\text{VO}(7,8\text{-dhf})_2]^{2-}$  is oriented outside (*cf.* **Figure S6** with **Figure 6**).

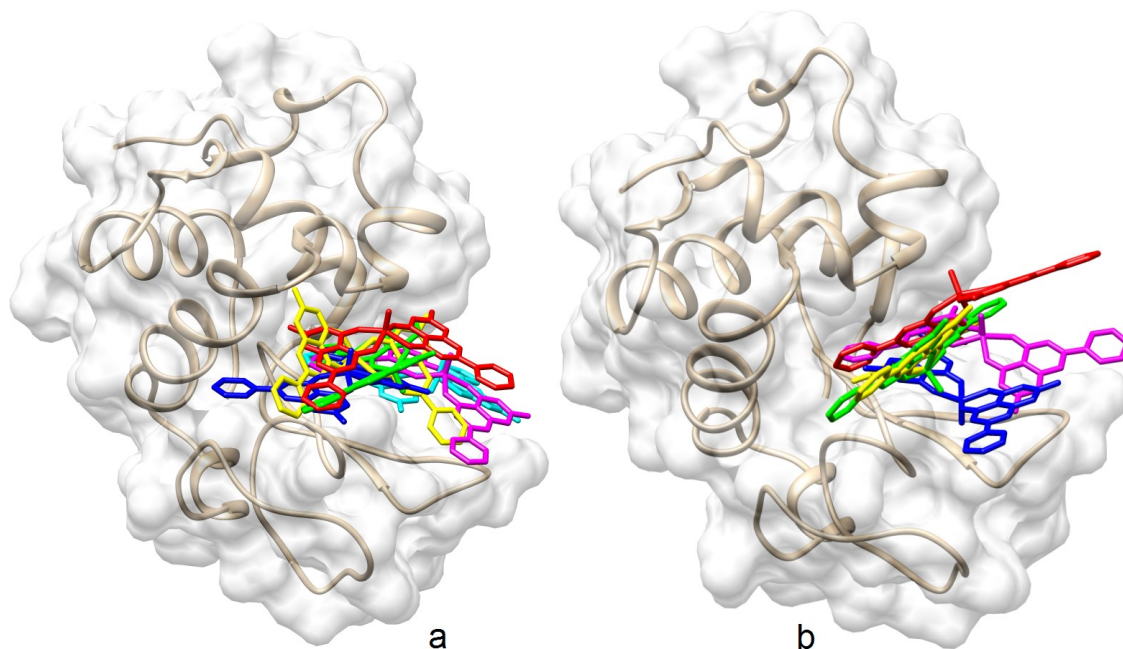


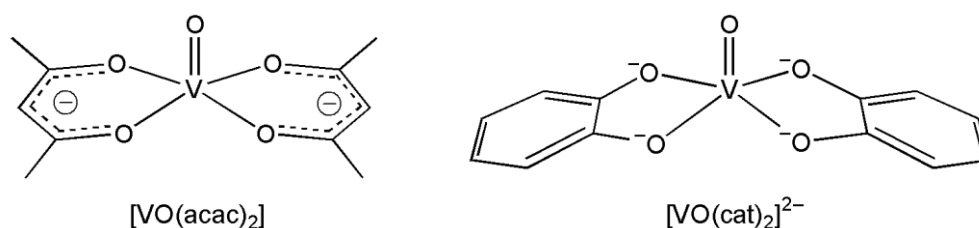
**Figure 7.** Cluster distribution for the interaction of lysozyme with the complexes *SPY-5-13*- $[\text{VO}(\text{chr})_2]$  (a), and *SPY-5-12*- $[\text{VO}(\text{chr})_2]$  (b). The six clusters for *SPY-5-13* and the five clusters for *SPY-5-12* isomer are represented with different colors.

The cluster distribution of the isomers *SPY-5-13* and *SPY-5-12* is reported in **Figure 7** with the different clusters shown with different colours. They are all concentrated in the cleft of the protein, but they are significantly scattered. This suggests a lack of specificity in the binding and, similarly to what observed for  $[\text{VO}(\text{que})_2]^{2-}$ ,  $[\text{VO}(\text{mor})_2]$  and  $[\text{VO}(7,8\text{-dhf})_2]^{2-}$ , it can be supposed a dynamic equilibrium between the various binding sites at the protein surface.

The EPR spectra of the  $\text{V}^{\text{IV}}\text{O}^{2+}/5\text{-hf}$  system are very similar to that described above for chrisin (**Figure S7 of Supporting Information**). In agreement with the EPR behavior, the docking calculations indicate that, for both the isomers *SPY-5-13* and *SPY-5-12*, the scoring *Fitness* values are lower than for the species of que, mor and 7,8-dhf and comparable with those of chr (**Table S3**).

For all the clusters, the strongest interaction is between the V=O and peptide NH group of Val109 or side-chain of Trp62, Trp63, and Arg112 (Table S3). Figure S8 illustrates the pose with highest *Fitness* and population for the interaction of the two isomers of [VO(5-hf)<sub>2</sub>] with lysozyme. Similarly to the solutions of [VO(chr)<sub>2</sub>], the V=O bond points toward the protein. The cluster distribution is shown in Figure S9. As found for [VO(chr)<sub>2</sub>], the most stable poses are in the cleft of the protein and indicate the presence of more than one binding site. This would suggest that [VO(5-hf)<sub>2</sub>], as a function of the time, binds to different residues around the cleft. On the basis of EPR data, which indicate that the spectrum is *slow-tumbling*, it can be inferred that this interaction is so weak that most of V exists in solution as free complex.

(4). Systems V<sup>IV</sup>O<sup>2+</sup>/acac/Lyz and V<sup>IV</sup>O<sup>2+</sup>/cat/Lyz. At physiological pH acetylacetonate(−) and catecholate(2−) form stable square pyramidal V<sup>IV</sup>O complexes with composition [VO(acac)<sub>2</sub>] and (CO, O<sup>−</sup>) coordination mode,<sup>49</sup> and [VO(cat)<sub>2</sub>]<sup>2−</sup> and (O<sup>−</sup>, O<sup>−</sup>) coordination mode,<sup>50</sup> respectively, as demonstrated by X-ray diffraction analysis. Since the ligands are symmetrical, no isomers are possible (Scheme 4).



**Scheme 4.** Structure of [VO(acac)<sub>2</sub>] and [VO(cat)<sub>2</sub>]<sup>2−</sup> species formed by acetylacetonate(−) and catecholate(2−) anions.

The EPR spectra recorded in the system containing V<sup>IV</sup>O<sup>2+</sup> ion, cat and lysozyme are shown in Figure 8, while those in the system with V<sup>IV</sup>O<sup>2+</sup> ion, acac and lysozyme in Figure S10 of Supporting



**Information.** It can be noticed that for these two systems, similarly to those with chr and 5-hf, the spectra recorded in the binary and ternary system are identical, suggesting that the interaction with the protein is very weak. In contrast with chr and 5-hf, the spectra are not of the *slow-tumbling* type and are perfectly *isotropic*.

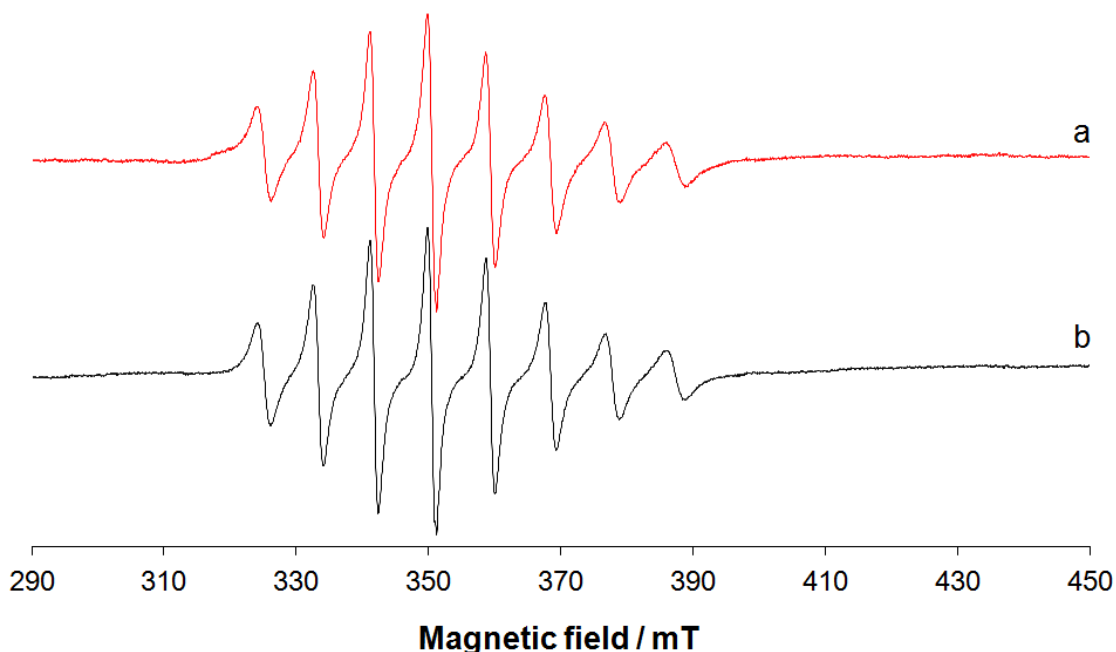


**Figure 8.** X-band EPR spectra recorded at pH 7.40 on: a) ternary system  $V^{IV}O^{2+}/cat/Lyz$  1/2/1 at 298 K and  $\nu = 9.853$  GHz ( $V^{IV}O^{2+}$  concentration  $7.0 \times 10^{-4}$  M) and b) binary system  $V^{IV}O^{2+}/cat$  1/2 at 298 K and  $\nu = 9.853$  GHz ( $V^{IV}O^{2+}$  concentration  $7.0 \times 10^{-4}$  M).

For  $[VO(cat)]^{2-}$ , GOLD predicts a very low binding affinity for all the solutions found in the four clusters, with the first being the more populated. The absence of *hbond* donors/acceptors groups and the limited possibility to form *vdW* interactions determine the very low value of  $F_{max}$ . From the data in **Table 3**, it emerges that the only polar residue involved in the interaction is tryptophan (Trp62, Trp63). The best pose is shown in **Figure 9**, while the cluster distribution is illustrated in **Figure S11 of Supporting Information**.

**Table 3.** Docking results of the interaction of  $[\text{VO}(\text{cat})_2]^{2-}$  with lysozyme.<sup>a</sup>

Cluster	Interacting residue	Distance O...X <sup>c</sup>	$F_{\text{max}}$ <sup>d</sup>	$F_{\text{mean}}$ <sup>e</sup>	Pop. <sup>f</sup>
I cluster	VO <sub>1</sub> ...Trp63(NH)	1.945	10.63	10.39	81/100
II cluster	VO <sub>1</sub> ...Trp63(NH)	1.674	10.57	10.36	6/100
III cluster	VO <sub>1</sub> ...Trp63(NH)	1.884	10.51	10.35	7/100
IV cluster	VO <sub>1</sub> ...Trp62(NH)	2.063	10.01	10.00	2/100

<sup>a</sup> Structure of  $[\text{VO}(\text{cat})_2]^{2-}$  simulated with Gaussian 09 at the level of theory B3P86/6-311g. <sup>b</sup> In the table only the clusters with the highest *Fitness* value are reported. <sup>c</sup> Distance in Å. <sup>d</sup> *Fitness* value for the most stable pose of each cluster ( $F_{\text{max}}$ ). <sup>e</sup> Mean *Fitness* value of the GoldScore scoring function for each cluster ( $F_{\text{mean}}$ ). <sup>f</sup> Number of solutions in the identified cluster.

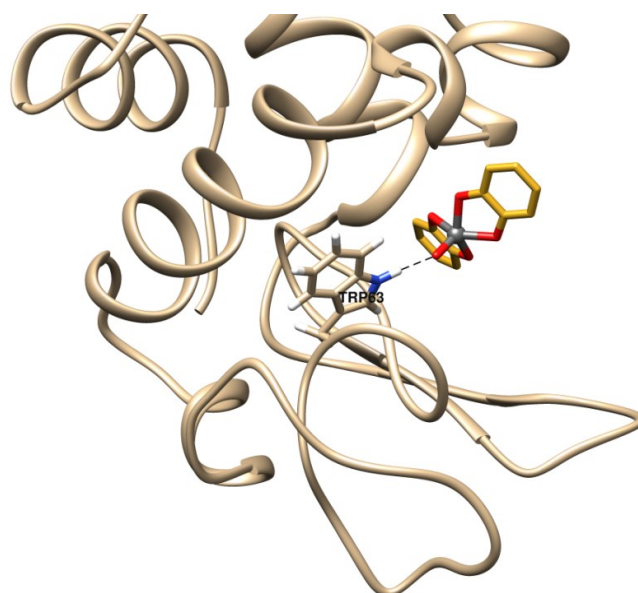


**Figure 9.** The most stable pose predicted by GOLD 5.2 for the adduct formed by  $[\text{VO}(\text{cat})_2]^{2-}$  with lysozyme.

The results obtained with  $[\text{VO}(\text{acac})_2]$  are reported in **Table S4 of Supporting Information** (docking data for the interaction with lysozyme) and **Figure S12** (best pose for the adduct formed with lysozyme). In perfect analogy with the complex formed by catecholate, the docking simulations predict a large cluster for the binding of  $[\text{VO}(\text{acac})_2]$  to lysozyme with very low affinity. For this only solution an *hbond* interaction between the VO and NH group of Trp63 residue is predicted (**Figure S12**).

**(5). Rationalization of the data.** The experimental results discussed in the previous sections present a gradual variation of the EPR spectra which can be related to the strength of the interaction between the square pyramidal complexes  $\text{VOL}_2$  and the accessible residues on the lysozyme surface. In particular, the spectra recorded at room temperature are *rigid limit* for  $[\text{VO}(\text{que})_2]^{2-}$  and  $[\text{VO}(\text{mor})_2]$  (Figures 1 and S1 of Supporting Information), *rigid limit* but with *isotropic* resonances for  $[\text{VO}(7,8\text{-dhf})_2]^{2-}$  (Figure 5), of the *slow tumbling* type for  $[\text{VO}(\text{chr})_2]$  and  $[\text{VO}(5\text{-hf})_2]$  (Figures S5 and S7), and *isotropic* for  $[\text{VO}(\text{acac})_2]$  and  $[\text{VO}(\text{cat})_2]^{2-}$  (Figures 8 and S10). On the basis of these results, the order of strength of the interaction can be summarized in this manner:  $[\text{VO}(\text{que})_2]^{2-} \sim [\text{VO}(\text{mor})_2] > [\text{VO}(7,8\text{-dhf})_2]^{2-} > [\text{VO}(\text{chr})_2] \sim [\text{VO}(5\text{-hf})_2] > [\text{VO}(\text{acac})_2] \sim [\text{VO}(\text{cat})_2]^{2-}$ .

The docking calculations allowed us to rationalize the EPR data through the evaluation of the GoldScore scoring function  $F$  and, in particular, of the terms related to the *hbond* and *vdW* intermolecular interactions ( $S_{\text{hbond}}^{\text{ext}}$  and  $S_{\text{vdW}}^{\text{ext}}$ , respectively, in eq. 1). The results are reported in Table 4.

**Table 4.** Docking parameters for  $\text{V}^{\text{IV}}\text{O}$  complexes examined in this study.

$\text{V}^{\text{IV}}\text{O}$ complex	Isomer	EPR spectrum in the ternary system	Free OH / CO groups	$F_{\text{max}}$ <sup>a</sup>	Range of $F_{\text{mean}}$ <sup>b</sup>	$S_{\text{hbond}}^{\text{ext}}$ <sup>c</sup>	$0.3 \times S_{\text{vdW}}^{\text{ext}}$ <sup>d</sup>
[VO(mor) <sub>2</sub> ]	SPY-5-13	<i>rigid limit</i>	4 / 0	22.66	18.61-21.32	14.72	8.09
	SPY-5-12		4 / 0	21.52	16.62-19.33	13.18	8.74
[VO(que) <sub>2</sub> ] <sup>2-</sup>	SPY-5-13	<i>rigid limit</i>	3 / 1	21.95	18.13-21.26	15.21	6.91
	SPY-5-12		3 / 1	19.47	17.63-18.96	12.49	7.29
[VO(7,8-dhf) <sub>2</sub> ] <sup>2-</sup>	SPY-5-13	<i>rigid limit</i> with <i>isotropic</i> resonances	0 / 1	17.16	14.68-16.49	11.92	5.24
	SPY-5-12		0 / 1	16.97	16.34	11.87	5.10

[VO(chr) <sub>2</sub> ]	SPY-5-13	Slow-tumbling	1 / 0	15.90	14.18-14.87	6.00	9.96
	SPY-5-12		1 / 0	15.49	13.03-14.31	6.56	9.33
[VO(5-hf) <sub>2</sub> ]	SPY-5-13	Slow-tumbling	0 / 0	15.97	13.57-14.59	6.00	9.97
	SPY-5-12		0 / 0	13.80	11.93-13.08	6.00	7.80
[VO(acac) <sub>2</sub> ]	e	Isotropic	0 / 0	12.50	–	6.00	2.94
[VO(cat) <sub>2</sub> ] <sup>2-</sup>	e	Isotropic	0 / 0	10.36	10.00-10.39	6.00	4.63

<sup>a</sup> *Fitness* value of the GoldScore scoring function (see eq. 1) for the most stable pose of each cluster ( $F_{\max}$ ). <sup>b</sup> Range of the mean *Fitness* value of the GoldScore scoring function (see eq. 1) for each cluster ( $F_{\text{mean}}$ ). <sup>c</sup> Scoring term related to the intermolecular *hbond*. <sup>d</sup> Scoring term related to the *vdW* intermolecular interactions. <sup>e</sup> Only one isomer is possible.

The data can be ordered on the basis of the values of the GoldScore scoring function  $F_{\max}$  (scoring of the most stable pose of the cluster) or  $F_{\text{mean}}$  (mean scoring value of the cluster).  $F_{\max}$  (see eq. 1) consists of the contributions of the hydrogen bond and van der Waals terms; for [VO(mor)<sub>2</sub>], [VO(que)<sub>2</sub>]<sup>2-</sup> and [VO(7,8-dhf)<sub>2</sub>]<sup>2-</sup>  $S_{\text{hbond}}^{\text{ext}}$  is larger than  $S_{\text{vdW}}^{\text{ext}}$  (approximately twice), while for the other four compounds the opposite trend is predicted. A value of  $F_{\max}$  in the range 16-17 marks the transition from a **rigid limit** (strong interaction with all V<sup>IV</sup>O species bound on the protein surface) to a *slow tumbling* or an *isotropic* (weak or no interaction with most of V<sup>IV</sup>O complex unbound and free to rotate in solution) EPR spectrum. Such a transition is easily observable comparing the spectra of the systems V<sup>IV</sup>O<sup>2+</sup>/7,8-dhf/Lyz and V<sup>IV</sup>O<sup>2+</sup>/chr/Lyz (cfr. Figure 5 and S5 of Supporting Information). The value of  $S_{\text{hbond}}^{\text{ext}}$ , and hence of  $F_{\max}$ , follows the number of free OH or CO groups (i.e. groups not involved in the V<sup>IV</sup>O<sup>2+</sup> binding) on the structure of the ligands: these are four in the ligands which give the strongest interaction (que and mor) and none in those which do not show interaction (5-hf, acac and que). Interestingly, 7,8-dhf and chr – which have one group potentially able to form intermolecular hydrogen bonds (CO for 7,8-dhf and OH for chr) – give a different spectrum, **rigid limit** in the first case and *slow-tumbling* in the second one (cfr. trace b of Figure 5 and trace a of Figure S5); this would suggest that for these ligands the presence of a C=O instead of O–H group favors the interaction of the V<sup>IV</sup>O complex with the surface residues.

However, besides the groups which could give *hbond* or *vdW* contacts, also the shape and size of the complex have certainly a role in determining the mode of interaction with the surface protein residues.

## Conclusions

The interaction with the proteins influences the transport, uptake and mechanism of action of metal species with pharmacological action. Two types of binding are expected for a metal complexes formed by an organic ligand L: i) a *covalent* binding, where the protein replaces with one of more amino acid residues the ligand L or a weak coordinated molecule, such as water, forming one or more coordination bonds and ii) a *non-covalent* binding, where the metal complex interacts through secondary interactions, such as van der Waals and hydrogen contacts, with the accessible groups on the protein surface.

V<sup>IV</sup>O complexes are known in the literature for their antidiabetic and antitumor properties. For *cis*-[VOL<sub>2</sub>(H<sub>2</sub>O)] compounds, where L is a bidentate monoanionic ligand, the proteins replace the water ligand with His-N or Asp/Glu-COO residues. This *covalent* interaction was discussed recently by our group through the combination of EPR and computational (docking and QM/MM) techniques.<sup>24</sup> The study of *non-covalent* interactions is probably more complicated and the combined application of several techniques – such as EPR, ESEEM, ENDOR, UV-Vis and CD spectroscopy, gel-electrophoresis, MALDI-TOF, SAXS, size-exclusion chromatography, polarography and voltammetry – is necessary.

In this work, a combination of EPR and docking techniques was applied to study the interaction between square pyramidal VOL<sub>2</sub> complexes (some of them with potential anticancer application) and lysozyme. All the complexes examined here are thermodynamically stable at physiological pH, but an interaction of VOL<sub>2</sub> with the residues on the protein surface could take place. EPR

spectroscopy gives a good description of the strength of such an interaction because at room temperature a *rigid limit* spectrum is expected when the *non-covalent* binding is strong enough to block the metal species on the protein surface (hindering the rotational motion in the EPR timescale) and a *slow-tumbling* or an *isotropic* spectrum when the binding is weak and the complexes are free to rotate in solution.

Docking methods provide valuable insights into the possible binding sites of V species on the protein surface. Comparing the computational with EPR data, we were able to find a good indicator to measure the strength of this interaction., i.e. the scoring of the most stable pose of the cluster  $F_{\max}$ , which allows to mark the transition from a *rigid limit* (strong interaction) to a *slow tumbling* or an *isotropic* (weak or no interaction) EPR spectrum. Carefully working under the limitation of the docking capabilities (i.e. scoring function validity for surface interactions), we could establish a chemically relevant hypothesis for this relative affinity. We suggest that it is function of the number of OH or CO groups, present in the ligand structure and not involved in the  $V^{IV}O^{2+}$  binding, able to form hydrogen bonds with the polar groups on the protein surface. Moreover, our results can be explained postulating a dynamical equilibrium between the various binding sites with the V species which distribute among such sites (giving a *rigid limit* EPR spectrum) and in aqueous solution (where they are free to rotate giving a *slow tumbling* or *isotropic* spectrum).

Overall, the results obtained with this EPR-docking strategy shed light on the interaction of V species and proteins when no coordination bounds are formed. We believe that this integrative spectroscopic and computational approach could be generalized to other metal complex systems, replacing the information of EPR spectroscopy with those of other instrumental/spectroscopic techniques and lysozyme with other proteins.

## Supporting Information

Tables with docking results for [VO(mor)<sub>2</sub>], [VO(chr)<sub>2</sub>], [VO(5-hf)<sub>2</sub>] and [VO(acac)<sub>2</sub>] (Tables S1-S4), figures with the EPR spectra of the systems V<sup>IV</sup>O<sup>2+</sup>/mor/Lyz, V<sup>IV</sup>O<sup>2+</sup>/chr/Lyz, V<sup>IV</sup>O<sup>2+</sup>/5-hf/Lyz and V<sup>IV</sup>O<sup>2+</sup>/acac/Lyz (Figures S1, S5, S7, S10), with the cluster distribution for the interaction of lysozyme with [VO(mor)<sub>2</sub>], [VO(7,8-dhf)<sub>2</sub>]<sup>2-</sup>, [VO(5-hf)<sub>2</sub>] and [VO(cat)<sub>2</sub>]<sup>2-</sup> (Figures S2, S4, S9, S11), with the most stable pose predicted for [VO(mor)<sub>2</sub>], [VO(chr)<sub>2</sub>], [VO(5-hf)<sub>2</sub>] and [VO(acac)<sub>2</sub>] (Figures S3, S6, S8, S12), and examples of input and output files of GOLD 5.2.

### **Acknowledgments**

J-D.M., A.L. and G.S. are thankful for the support given by the Spanish grant CTQ2017-87889-P and the Generalitat de Catalunya grant 2014SGR989. Support of COST Action CM1306 is kindly acknowledged. G.S. thanks the Universitat Autònoma de Barcelona for its support to his Ph.D. grant. D.S., V.U. and E.G. thank Fondazione di Sardegna (project FdS15Garribba) for the financial support.

## References

1. (a) Costa Pessoa, J.; Tomaz, I. Transport of therapeutic vanadium and ruthenium complexes by blood plasma components. *Curr. Med. Chem.* **2010**, *17*, 3701-3738. (b) Rehder, D. Vanadium. Its Role for Humans. In *Interrelations between Essential Metal Ions and Human Diseases*; Sigel, A., Sigel, H., Sigel, R. K. O., Ed.; Springer Science+Business Media: Dordrecht, 2013; pp 139-169. (c) Costa Pessoa, J.; Etcheverry, S.; Gambino, D. Vanadium compounds in medicine. *Coord. Chem. Rev.* **2015**, *301-302*, 24-48. (d) Rehder, D. Perspectives for vanadium in health issues. *Future Med. Chem.* **2016**, *8*, 325-338. (e) Leon, I. E.; Cadavid-Vargas, J. F.; Di Virgilio, A. L.; Etcheverry, S. B. Vanadium, ruthenium and copper compounds: a new class of nonplatinum metallodrugs with anticancer activity. *Curr. Med. Chem.* **2017**, *24*, 112-148.
2. (a) Sakurai, H.; Yoshikawa, Y.; Yasui, H. Current state for the development of metallopharmaceuticals and anti-diabetic metal complexes. *Chem. Soc. Rev.* **2008**, *37*, 2383-2392. (b) Thompson, K. H.; Orvig, C. Vanadium in diabetes: 100 years from Phase 0 to Phase I. *J. Inorg. Biochem.* **2006**, *100*, 1925-1935.
3. (a) Thompson, K. H.; Lichter, J.; LeBel, C.; Scaife, M. C.; McNeill, J. H.; Orvig, C. Vanadium treatment of type 2 diabetes: A view to the future. *J. Inorg. Biochem.* **2009**, *103*, 554-558. (b) Scior, T.; Guevara-Garcia, J. A.; Do, Q.-T.; Bernard, P.; Laufer, S. Why antidiabetic vanadium complexes are not in the pipeline of "big pharma" drug research? A critical review. *Curr. Med. Chem.* **2016**, *23*, 2874-2891. (c) Crans, D., C.; Yang, L.; Haase, A.; Yang, X. Health benefits of vanadium and its potential as an anticancer agent. In *Metal Ions in Life Sciences*; De Gruyter GmbH: Berlin, 2018; Vol. 18, pp 251-279.
4. Doucette, K. A.; Hassell, K. N.; Crans, D. C. Selective speciation improves efficacy and lowers toxicity of platinum anticancer and vanadium antidiabetic drugs. *J. Inorg. Biochem.* **2016**, *165*, 56-70.
5. Levina, A.; Crans, D. C.; Lay, P. A. Speciation of metal drugs, supplements and toxins in media and bodily fluids controls *in vitro* activities. *Coord. Chem. Rev.* **2017**, *352*, 473-498.
6. (a) Jakusch, T.; Kiss, T. *In vitro* study of the antidiabetic behavior of vanadium compounds. *Coord. Chem. Rev.* **2017**, *351*, 118-126. (b) Kiss, T.; Enyedy, É. A.; Jakusch, T. Development of the application of speciation in chemistry. *Coord. Chem. Rev.* **2017**, *352*, 401-423.
7. Yoshikawa, Y.; Sakurai, H.; Crans, D. C.; Micera, G.; Garribba, E. Structural and redox requirements for the action of anti-diabetic vanadium compounds. *Dalton Trans.* **2014**, *43*, 6965-6972.



8. (a) Sanna, D.; Micera, G.; Garribba, E. On the transport of vanadium in blood serum. *Inorg. Chem.* **2009**, *48*, 5747-5757. (b) Sanna, D.; Micera, G.; Garribba, E. New developments in the comprehension of the biotransformation and transport of insulin-enhancing vanadium compounds in the blood serum. *Inorg. Chem.* **2010**, *49*, 174-187. (c) Sanna, D.; Buglyó, P.; Micera, G.; Garribba, E. A quantitative study of the biotransformation of insulin-enhancing  $\text{VO}^{2+}$  compounds. *JBIC, J. Biol. Inorg. Chem.* **2010**, *15*, 825-839. (d) Sanna, D.; Micera, G.; Garribba, E. Interaction of  $\text{VO}^{2+}$  ion and some insulin-enhancing compounds with immunoglobulin G. *Inorg. Chem.* **2011**, *50*, 3717-3728. (e) Sanna, D.; Biro, L.; Buglyo, P.; Micera, G.; Garribba, E. Biotransformation of BMOV in the presence of blood serum proteins. *Metallomics* **2012**, *4*, 33-36. (f) Sanna, D.; Ugone, V.; Micera, G.; Garribba, E. Temperature and solvent structure dependence of  $\text{VO}^{2+}$  complexes of pyridine-N-oxide derivatives and their interaction with human serum transferrin. *Dalton Trans.* **2012**, *41*, 7304-7318. (g) Sanna, D.; Bíró, L.; Buglyó, P.; Micera, G.; Garribba, E. Transport of the anti-diabetic  $\text{VO}^{2+}$  complexes formed by pyrone derivatives in the blood serum. *J. Inorg. Biochem.* **2012**, *115*, 87-99. (h) Sanna, D.; Micera, G.; Garribba, E. Interaction of anti-diabetic vanadium compounds with human serum holo-transferrin. *Inorg. Chem.* **2013**, *52*, 11975-11985. (i) Koleša-Dobravec, T.; Lodyga-Chruscinska, E.; Symonowicz, M.; Sanna, D.; Meden, A.; Perdih, F.; Garribba, E. Synthesis and characterization of  $\text{V}^{\text{IV}}\text{O}$  complexes of picolinate and pyrazine derivatives. Behavior in the solid state and aqueous solution and biotransformation in the presence of blood plasma proteins. *Inorg. Chem.* **2014**, *53*, 7960-7976. (j) Sanna, D.; Ugone, V.; Micera, G.; Pivetta, T.; Valletta, E.; Garribba, E. Speciation of the potential antitumor agent vanadocene dichloride in the blood plasma and model systems. *Inorg. Chem.* **2015**, *54*, 8237-8250. (k) Sanna, D.; Ugone, V.; Pisano, L.; Serra, M.; Micera, G.; Garribba, E. Behavior of the potential antitumor  $\text{V}^{\text{IV}}\text{O}$  complexes formed by flavonoid ligands. 2. Characterization of sulfonate derivatives of quercetin and morin, interaction with the bioligands of the plasma and preliminary biotransformation studies. *J. Inorg. Biochem.* **2015**, *153*, 167-177. (l) Sanna, D.; Serra, M.; Ugone, V.; Manca, L.; Pirastru, M.; Buglyo, P.; Biro, L.; Micera, G.; Garribba, E. Biorelevant reactions of the potential anti-tumor agent vanadocene dichloride. *Metallomics* **2016**, *8*, 532-541. (m) Sanna, D.; Ugone, V.; Micera, G.; Buglyo, P.; Biro, L.; Garribba, E. Speciation in human blood of Metvan, a vanadium based potential anti-tumor drug. *Dalton Trans.* **2017**, *46*, 8950-8967. (n) Sanna, D.; Ugone, V.; Serra, M.; Garribba, E. Speciation of potential anti-diabetic vanadium complexes in real serum samples. *J. Inorg. Biochem.* **2017**, *173*, 52-65. (o) Sanna, D.; Ugone, V.; Sciortino, G.; Buglyo, P.; Bihari, Z.; Parajdi-Losonczy, P. L.; Garribba, E.  $\text{V}^{\text{IV}}\text{O}$  complexes with antibacterial quinolone ligands and their interaction with serum proteins. *Dalton Trans.* **2018**, *47*, 2164-2182.

9. (a) Willsky, G. R.; Goldfine, A. B.; Kostyniak, P. J.; McNeill, J. H.; Yang, L. Q.; Khan, H. R.; Crans, D. C. Effect of vanadium(IV) compounds in the treatment of diabetes: *in vivo* and *in vitro* studies with vanadyl sulfate and bis(maltolato)oxovanadium(IV). *J. Inorg. Biochem.* **2001**, *85*, 33-42. (b) Liboiron, B. D.; Thompson, K. H.; Hanson, G. R.; Lam, E.; Aebischer, N.; Orvig, C. New insights into the interactions of serum proteins with bis(maltolato)oxovanadium(IV): Transport and biotransformation of insulin-enhancing vanadium pharmaceuticals. *J. Am. Chem. Soc.* **2005**, *127*, 5104-5115. (c) Jakusch, T.; Hollender, D.; Enyedy, E. A.; Gonzalez, C. S.; Montes-Bayon, M.; Sanz-Medel, A.; Costa Pessoa, J.; Tomaz, I.; Kiss, T. Biospeciation of various antidiabetic V<sup>IV</sup>O compounds in serum. *Dalton Trans.* **2009**, 2428-2437. (d) Jakusch, T.; Costa Pessoa, J.; Kiss, T. The speciation of vanadium in human serum. *Coord. Chem. Rev.* **2011**, *255*, 2218-2226. (e) Correia, I.; Jakusch, T.; Cobbinna, E.; Mehtab, S.; Tomaz, I.; Nagy, N. V.; Rockenbauer, A.; Costa Pessoa, J.; Kiss, T. Evaluation of the binding of oxovanadium(IV) to human serum albumin. *Dalton Trans.* **2012**, *41*, 6477-6487. (f) Gonçalves, G.; Tomaz, A. I.; Correia, I.; Veiros, L. F.; Castro, M. M. C. A.; Avecilla, F.; Palacio, L.; Maestro, M.; Kiss, T.; Jakusch, T.; Garcia, M. H. V.; Costa Pessoa, J. A novel V<sup>IV</sup>O-pyrimidinone complex: synthesis, solution speciation and human serum protein binding. *Dalton Trans.* **2013**, *42*, 11841-11861. (g) Mehtab, S.; Gonçalves, G.; Roy, S.; Tomaz, A. I.; Santos-Silva, T.; Santos, M. F. A.; Romão, M. J.; Jakusch, T.; Kiss, T.; Costa Pessoa, J. Interaction of vanadium(IV) with human serum apotransferrin. *J. Inorg. Biochem.* **2013**, *121*, 187-195. (h) Costa Pessoa, J.; Gonçalves, G.; Roy, S.; Correia, I.; Mehtab, S.; Santos, M. F. A.; Santos-Silva, T. New insights on vanadium binding to human serum transferrin. *Inorg. Chim. Acta* **2014**, *420*, 60-68. (i) Santos, M. F. A.; Correia, I.; Oliveira, A. R.; Garribba, E.; Costa Pessoa, J.; Santos-Silva, T. Vanadium complexes as prospective therapeutics: Structural characterization of a V<sup>IV</sup> lysozyme adduct. *Eur. J. Inorg. Chem.* **2014**, 3293-3297.
10. Costa Pessoa, J.; Garribba, E.; Santos, M. F. A.; Santos-Silva, T. Vanadium and proteins: Uptake, transport, structure, activity and function. *Coord. Chem. Rev.* **2015**, *301-302*, 49-86.
11. (a) Sanna, D.; Serra, M.; Micera, G.; Garribba, E. Interaction of antidiabetic vanadium compounds with hemoglobin and red blood cells and their distribution between plasma and erythrocytes. *Inorg. Chem.* **2014**, *53*, 1449-1464. (b) Sanna, D.; Serra, M.; Micera, G.; Garribba, E. Uptake of potential anti-diabetic V<sup>IV</sup>O compounds of picolinate ligands by red blood cells. *Inorg. Chim. Acta* **2014**, *420*, 75-84.
12. Crans, D. C.; Smee, J. J.; Gaidamauskas, E.; Yang, L. The chemistry and biochemistry of vanadium and the biological activities exerted by vanadium compounds. *Chem. Rev.* **2004**, *104*, 849-902.

13. Rehder, D. *Bioinorganic Vanadium Chemistry*. John Wiley & Sons, Ltd: Chichester, 2008.
14. (a) Dias, D. M.; Rodrigues, J. P. G. L. M.; Domingues, N. S.; Bonvin, A. M. J. J.; Castro, M. M. C. A. Unveiling the interaction of vanadium Compounds with human serum albumin by using  $^1\text{H}$  STD NMR and computational docking studies. *Eur. J. Inorg. Chem.* **2013**, *2013*, 4619-4627. (b) Martins, P. G. A.; Mori, M.; Chiaradia-Delatorre, L. D.; Menegatti, A. C. O.; Mascarello, A.; Botta, B.; Benítez, J.; Gambino, D.; Terenzi, H. Exploring oxidovanadium(IV) complexes as YopH inhibitors: Mechanism of action and modeling studies. *ACS Med. Chem. Lett.* **2015**, *6*, 1035-1040. (c) Scalese, G.; Benítez, J.; Rostán, S.; Correia, I.; Bradford, L.; Vieites, M.; Minini, L.; Merlino, A.; Coitiño, E. L.; Birriel, E.; Varela, J.; Cerecetto, H.; González, M.; Costa Pessoa, J.; Gambino, D. Expanding the family of heteroleptic oxidovanadium(IV) compounds with salicylaldehyde semicarbazones and polypyridyl ligands showing anti-*Trypanosoma cruzi* activity. *J. Inorg. Biochem.* **2015**, *147*, 116-125.
15. Correia, I.; Chorna, I.; Cavaco, I.; Roy, S.; Kuznetsov, M. L.; Ribeiro, N.; Justino, G.; Marques, F.; Santos-Silva, T.; Santos, M. F. A.; Santos, H. M.; Capelo, J. L.; Douth, J.; Costa Pessoa, J. Interaction of  $[\text{V}^{\text{IV}}\text{O}(\text{acac})_2]$  with human serum transferrin and albumin. *Chem. Asian J.* **2017**, *12*, 2062-2084.
16. (a) Eaton, S. S.; Dubach, J.; More, K. M.; Eaton, G. R.; Thurman, G.; Ambruso, D. R. Comparison of the electron spin echo envelope modulation (ESEEM) for human lactoferrin and transferrin complexes of copper(II) and vanadyl ion. *J. Biol. Chem.* **1989**, *264*, 4776-81. (b) Gerfen, G. J.; Hanna, P. M.; Chasteen, N. D.; Singel, D. J. Characterization of the ligand environment of vanadyl complexes of apoferritin by multifrequency electron spin-echo envelope modulation. *J. Am. Chem. Soc.* **1991**, *113*, 9513-9519.
17. Hanna, P. M.; Chasteen, N. D.; Rottman, G. A.; Aisen, P. Iron binding to horse spleen apoferritin: a vanadyl ENDOR spin probe study. *Biochemistry* **1991**, *30*, 9210-9216.
18. Smith, C. A.; Ainscough, E. W.; Brodie, A. M. Complexes of human lactoferrin with vanadium in oxidation states +3, +4 and +5. *J. Chem. Soc., Dalton Trans.* **1995**, 1121-1126.
19. Azevedo, C. G.; Correia, I.; dos Santos, M. M. C.; Santos, M. F. A.; Santos-Silva, T.; Douth, J.; Fernandes, L.; Santos, H. M.; Capelo, J. L.; Costa Pessoa, J. Binding of vanadium to human serum transferrin - voltammetric and spectrometric studies. *J. Inorg. Biochem.* **2018**, *180*, 211-221.
20. In docking terminology the species that interacts with the protein is named ligand. This term could generate confusion when the ligand is a metal complex; therefore, when it refers to the terminology used in the docking studies, it will be written in italic in the text.

21. Ortega-Carrasco, E.; Lledós, A.; Maréchal, J.-D. Assessing protein–ligand docking for the binding of organometallic compounds to proteins. *J. Comput. Chem.* **2014**, *35*, 192-198.
22. Robles, V. M.; Dürrenberger, M.; Heinisch, T.; Lledós, A.; Schirmer, T.; Ward, T. R.; Maréchal, J.-D. Structural, kinetic, and docking studies of artificial imine reductases based on biotin–streptavidin technology: An induced lock-and-key hypothesis. *J. Am. Chem. Soc.* **2014**, *136*, 15676-15683.
23. Sciortino, G.; Rodríguez-Guerra Pedregal, J.; Lledós, A.; Garribba, E.; Maréchal, J.-D. Prediction of the interaction of metallic moieties with proteins: An update for protein-ligand docking techniques. *J. Comput. Chem.* **2018**, *39*, 42-51.
24. Sciortino, G.; Sanna, D.; Ugone, V.; Micera, G.; Lledós, A.; Maréchal, J.-D.; Garribba, E. Elucidation of binding site and chiral specificity of oxidovanadium drugs with lysozyme through theoretical calculations. *Inorg. Chem.* **2017**, *56*, 12938-12951.
25. (a) Barrio, D. A.; Etcheverry, S. B. Potential use of vanadium compounds in therapeutics. *Curr. Med. Chem.* **2010**, *17*, 3632-3642. (b) Ferrer, E.; Salinas, M.; Correa, M.; Naso, L.; Barrio, D.; Etcheverry, S.; Lezama, L.; Rojo, T.; Williams, P. M. Synthesis, characterization, antitumoral and osteogenic activities of quercetin vanadyl(IV) complexes. *JBIC, J. Biol. Inorg. Chem.* **2006**, *11*, 791-801. (c) Naso, L. G.; Lezama, L.; Rojo, T.; Etcheverry, S. B.; Valcarcel, M.; Roura, M.; Salado, C.; Ferrer, E. G.; Williams, P. A. M. Biological evaluation of morin and its new oxovanadium(IV) complex as anti-oxidant and specific anti-cancer agents. *Chem.-Biol. Interact.* **2013**, *206*, 289-301. (d) León, I. E.; Cadavid-Vargas, J. F.; Tiscornia, I.; Porro, V.; Castelli, S.; Katkar, P.; Desideri, A.; Bollati-Fogolin, M.; Etcheverry, S. B. Oxidovanadium(IV) complexes with chrysin and silibinin: anticancer activity and mechanisms of action in a human colon adenocarcinoma model. *JBIC, J. Biol. Inorg. Chem.* **2015**, *20*, 1175-1191. (e) León, I. E.; Cadavid-Vargas, J. F.; Resasco, A.; Maschi, F.; Ayala, M. A.; Carbone, C.; Etcheverry, S. B. *In vitro* and *in vivo* antitumor effects of the VO-chrysin complex on a new three-dimensional osteosarcoma spheroids model and a xenograft tumor in mice. *JBIC, J. Biol. Inorg. Chem.* **2016**, *21*, 1009-1020. (f) Leon, I. E.; Diez, P.; Etcheverry, S. B.; Fuentes, M. Deciphering the effect of an oxovanadium(IV) complex with the flavonoid chrysin (VOChrys) on intracellular cell signalling pathways in an osteosarcoma cell line. *Metallomics* **2016**, *8*, 739-749.
26. Wenzel, M.; Casini, A. Mass spectrometry as a powerful tool to study therapeutic metallodrugs speciation mechanisms: Current frontiers and perspectives. *Coord. Chem. Rev.* **2017**, *352*, 432-460.
27. (a) Amin, S. S.; Cryer, K.; Zhang, B.; Dutta, S. K.; Eaton, S. S.; Anderson, O. P.; Miller, S. M.; Reul, B. A.; Brichard, S. M.; Crans, D. C. Chemistry and insulin-mimetic properties of

bis(acetylacetonate)oxovanadium(IV) and derivatives1. *Inorg. Chem.* **2000**, *39*, 406-416. (b) Reul, B. A.; Amin, S. S.; Buchet, J.-P.; Ongemba, L. N.; Crans, D. C.; Brichard, S. M. Effects of vanadium complexes with organic ligands on glucose metabolism: a comparison study in diabetic rats. *Br. J. Pharmacol.* **1999**, *126*, 467-477. (c) Yang, X.-G.; Yang, X.-D.; Yuan, L.; Wang, K.; Crans, D. C. The permeability and cytotoxicity of insulin-mimetic vanadium compounds. *Pharm. Res.* **2004**, *21*, 1026-1033. (d) Fu, Y.; Wang, Q.; Yang, X.-G.; Yang, X.-D.; Wang, K. Vanadyl bisacetylacetonate induced G1/S cell cycle arrest via high-intensity ERK phosphorylation in HepG2 cells. *JBIC, J. Biol. Inorg. Chem.* **2008**, *13*, 1001. (e) Liu, J.-C.; Yu, Y.; Wang, G.; Wang, K.; Yang, X.-G. Bis(acetylacetonato)-oxovanadium(IV), bis(maltolato)-oxovanadium(IV) and sodium metavanadate induce antiproliferative effects by regulating hormone-sensitive lipase and perilipin via activation of Akt. *Metallomics* **2013**, *5*, 813-820. (f) Makinen, M. W.; Salehitazangi, M. The structural basis of action of vanadyl (VO<sup>2+</sup>) chelates in cells. *Coord. Chem. Rev.* **2014**, *279*, 1-22. (g) Wu, J.-X.; Hong, Y.-H.; Yang, X.-G. Bis(acetylacetonato)-oxidovanadium(IV) and sodium metavanadate inhibit cell proliferation via ROS-induced sustained MAPK/ERK activation but with elevated AKT activity in human pancreatic cancer AsPC-1 cells. *JBIC, J. Biol. Inorg. Chem.* **2016**, *21*, 919-929.

28. Frisch, M. J.; Trucks, G. W.; Schlegel, H. B.; Scuseria, G. E.; Robb, M. A.; Cheeseman, J. R.; Scalmani, G.; Barone, V.; Mennucci, B.; Petersson, G. A.; Nakatsuji, H.; Caricato, M. L., X.; Hratchian, H. P.; Izmaylov, A. F.; Bloino, J.; Zheng, G.; Sonnenberg, J. L.; Hada, M.; Ehara, M.; Toyota, K.; Fukuda, R.; Hasegawa, J.; Ishida, M.; Nakajima, T.; Honda, Y.; Kitao, O.; Nakai, H.; Vreven, T.; Montgomery, J. A., Jr.; Peralta, J. E.; Ogliaro, F.; Bearpark, M.; Heyd, J. J.; Brothers, E.; Kudin, K. N.; Staroverov, V. N.; Keith, T.; Kobayashi, R.; Normand, J.; Raghavachari, K.; Rendell, A.; Burant, J. C.; Iyengar, S. S.; Tomasi, J.; Cossi, M.; Rega, N.; Millam, J. M.; Klene, M.; Knox, J. E.; Cross, J. B.; Bakken, V.; Adamo, C. J., J.; Gomperts, R.; Stratmann, R. E.; Yazyev, O.; Austin, A. J.; Cammi, R.; Pomelli, C.; Ochterski, J. W.; Martin, R. L.; Morokuma, K.; Zakrzewski, V. G.; Voth, G. A.; Salvador, P.; Dannenberg, J. J.; Dapprich, S.; Daniels, A. D.; Farkas, Ö.; Foresman, J. B.; Ortiz, J. V.; Cioslowski, J.; Fox, D. J. *Gaussian 09, revision C.01*. Gaussian, Inc.: Wallingford, CT, 2009.

29. (a) Micera, G.; Garribba, E. The effect of the functional, basis set, and solvent in the simulation of the geometry and spectroscopic properties of V<sup>IV</sup>O<sup>2+</sup> complexes. chemical and biological applications. *Int. J. Quantum Chem.* **2012**, *112*, 2486-2498. (b) Micera, G.; Garribba, E. Application of DFT methods in the study of V<sup>IV</sup>O<sup>2+</sup>-peptide interactions. *Eur. J. Inorg. Chem.* **2010**, 4697-4710. (c) Micera, G.; Garribba, E. The effect of trigonal bipyramidal distortion of pentacoordinate V<sup>IV</sup>O<sup>2+</sup> species on their structural, electronic and spectroscopic parameters. *Eur. J.*

- Inorg. Chem.* **2011**, 3768-3780. (d) Sanna, D.; Varnágy, K.; Timári, S.; Micera, G.; Garribba, E. VO<sup>2+</sup> complexation by bioligands showing keto–enol tautomerism: A potentiometric, spectroscopic, and computational study. *Inorg. Chem.* **2011**, *50*, 10328-10341. (e) Sanna, D.; Buglyo, P.; Tomaz, A. I.; Costa Pessoa, J.; Borovic, S.; Micera, G.; Garribba, E. V<sup>IV</sup>O and Cu<sup>II</sup> complexation by ligands based on pyridine nitrogen donors. *Dalton Trans.* **2012**, *41*, 12824-12838. (f) Sanna, D.; Buglyó, P.; Bíró, L.; Micera, G.; Garribba, E. Coordinating properties of pyrone and pyridinone derivatives, tropolone and catechol toward the VO<sup>2+</sup> ion: An experimental and computational approach. *Eur. J. Inorg. Chem.* **2012**, 1079-1092. (g) Sanna, D.; Pecoraro, V.; Micera, G.; Garribba, E. Application of DFT methods to the study of the coordination environment of the VO<sup>2+</sup> ion in V proteins. *JBIC, J. Biol. Inorg. Chem.* **2012**, *17*, 773-790. (h) Sanna, D.; Várnagy, K.; Lihi, N.; Micera, G.; Garribba, E. Formation of new non-oxido vanadium(IV) species in aqueous solution and in the solid state by tridentate (O, N, O) ligands and rationalization of their EPR behavior. *Inorg. Chem.* **2013**, *52*, 8202-8213. (i) Pisano, L.; Varnagy, K.; Timári, S.; Hegetschweiler, K.; Micera, G.; Garribba, E. V<sup>IV</sup>O versus V<sup>IV</sup> complex formation by tridentate (O, N<sub>arom</sub>, O) ligands: Prediction of geometry, EPR <sup>51</sup>V hyperfine coupling constants, and UV–Vis spectra. *Inorg. Chem.* **2013**, *52*, 5260-5272.
30. (a) Bühl, M.; Kabrede, H. Geometries of transition-metal complexes from density-functional theory. *J. Chem. Theory Comput.* **2006**, *2*, 1282-1290. (b) Bühl, M.; Reimann, C.; Pantazis, D. A.; Bredow, T.; Neese, F. Geometries of third-row transition-metal complexes from density-functional theory. *J. Chem. Theory Comput.* **2008**, *4*, 1449-1459.
31. (a) Verdonk, M. L.; Cole, J. C.; Hartshorn, M. J.; Murray, C. W.; Taylor, R. D. Improved protein–ligand docking using GOLD. *Proteins: Struct., Funct., Bioinf.* **2003**, *52*, 609-623. (b) Jones, G.; Willett, P.; Glen, R. C. Molecular recognition of receptor sites using a genetic algorithm with a description of desolvation. *J. Mol. Biol.* **1995**, *245*, 43-53.
32. Diamond, R. Real-space refinement of the structure of hen egg-white lysozyme. *J. Mol. Biol.* **1974**, *82*, 371-391.
33. Berman, H. M.; Westbrook, J.; Feng, Z.; Gilliland, G.; Bhat, T. N.; Weissig, H.; Shindyalov, I. N.; Bourne, P. E. The Protein Data Bank. *Nucleic Acids Res.* **2000**, *28*, 235-242.
34. Pettersen, E. F.; Goddard, T. D.; Huang, C. C.; Couch, G. S.; Greenblatt, D. M.; Meng, E. C.; Ferrin, T. E. UCSF Chimera-A visualization system for exploratory research and analysis. *J. Comput. Chem.* **2004**, *25*, 1605-1612.
35. (a) Rodríguez-Guerra Pedregal, J. *Insilichem/gaudiview: Pre-alpha public releas, Zenodo*. 2017. (b) Rodríguez-Guerra Pedregal, J.; Sciortino, G.; Guasp, J.; Municoy, M.; Maréchal, J.-D. GaudiMM: A modular multi-objective platform for molecular modeling. *J. Comput. Chem.* **2017**, *38*, 2118-2126.

36. Nagypál, I.; Fábián, I. NMR relaxation studies in solution of transition metal complexes. V. Proton exchange reactions in aqueous solutions of  $\text{VO}^{2+}$ -oxalic acid, -malonic acid systems. *Inorg. Chim. Acta* **1982**, *61*, 109-113.
37. Sanna, D.; Ugone, V.; Lubinu, G.; Micera, G.; Garribba, E. Behavior of the potential antitumor  $\text{V}^{\text{IV}}\text{O}$  complexes formed by flavonoid ligands. 1. Coordination modes and geometry in solution and at the physiological pH. *J. Inorg. Biochem.* **2014**, *140*, 173-184.
38. *WINEPR SimFonia, version 1.25*. Bruker Analytische Messtechnik GmbH: Karlsruhe, 1996.
39. Chasteen, D. N. Vanadyl(IV) EPR spin probe. Inorganic and biochemical aspects. In *Biological Magnetic Resonance*; Berliner, L. J., Reuben, J., Ed.; Plenum Press: New York, 1981; Vol. 3, pp 53-119.
40. Smith II, T. S.; LoBrutto, R.; Pecoraro, V. L. Paramagnetic spectroscopy of vanadyl complexes and its applications to biological systems. *Coord. Chem. Rev.* **2002**, *228*, 1-18.
41. Garribba, E.; Lodyga-Chruscinska, E.; Micera, G.; Panzanelli, A.; Sanna, D. Binding of oxovanadium(IV) to dipeptides containing histidine and cysteine residues. *Eur. J. Inorg. Chem.* **2005**, 1369-1382.
42. (a) Forbes, M. D. E.; Jarocha, L. E.; Sim, S.; Tarasov, V. F. Time-resolved Electron Paramagnetic Resonance spectroscopy. *Adv. Phys. Org. Chem.* **2013**, *47*, 1-83. (b) Neshchadin, D.; Batchelor, S. N.; Bilkis, I.; Gescheidt, G. Short-lived phenoxyl radicals formed from green-tea polyphenols and highly reactive oxygen species: An investigation by time-resolved EPR spectroscopy. *Angew. Chem., Int. Ed.* **2014**, *53*, 13288-13292.
43. Campbell, R. F.; Freed, J. H. Slow-motional ESR spectra for vanadyl complexes and their model dependence. *J. Phys. Chem.* **1980**, *84*, 2668-2680.
44. *Nomenclature of Inorganic Chemistry – IUPAC Recommendations*. Connelly, N. G.; Damhus, T.; Hartshorn, R. M.; Hutton, A. T. Eds. The Royal Society of Chemistry: Cambridge, 2005. According to IUPAC nomenclature, the configuration index of square pyramidal (*SPY-5*) complexes consists of two digits: the first digit is the priority number of the donor on the  $C_4$  symmetry axis of the idealized pyramid, and the second digit is the priority number of the donor trans to that with the lowest priority number in the plane perpendicular to the  $C_4$  axis. The procedure for assigning priority numbers to the donor atoms is based upon the standard sequence rules developed for chiral carbon compounds by Cahn, Ingold and Prelog (CIP rules).
45. (a) Hagen, W. R. Dislocation strain broadening as a source of anisotropic linewidth and asymmetrical lineshape in the electron paramagnetic resonance spectrum of metalloproteins and related systems. *J. Magn. Reson.* **1981**, *44*, 447-469. (b) Hagen, W. R. Aqueous solutions. In *Biomolecular EPR Spectroscopy*; CRC Press: 2008; pp 169-180.

46. *Lysozymes: model enzymes in biochemistry and biology*. Jollès, P., Ed.; Birkhäuser Verlag: Basel, 1996.
47. Vocadlo, D. J.; Davies, G. J.; Laine, R.; Withers, S. G. Catalysis by hen egg-white lysozyme proceeds via a covalent intermediate. *Nature* **2001**, *412*, 835-838.
48. Dumoulin, M.; Johnson, R. J. K.; Bellotti, V.; Dobson, C. M. Human lysozyme. In *Protein misfolding, aggregation, and conformational diseases: Part B: molecular mechanisms of conformational diseases*; Uversky, V. N., Fink, A. L., Ed.; Springer US: Boston, MA, 2007; pp 285-308.
49. (a) Manabu, H.; Akiko, S.; Hidehiro, U.; Yuji, O. X-ray analysis of bond elongation in VO(acac)<sub>2</sub> at the excited state. *Chem. Lett.* **2005**, *34*, 1228-1229. (b) Shuter, E.; Rettig, S. J.; Orvig, C. Oxobis(2,4-pentanedionato)vanadium(IV), a redetermination. *Acta Crystallographica Section C* **1995**, *51*, 12-14.
50. Cooper, S. R.; Koh, Y. B.; Raymond, K. N. Synthetic, structural, and physical studies of bis(triethylammonium) tris(catecholato)vanadate(IV), potassium bis(catecholato)oxovanadate(IV), and potassium tris(catecholato)vanadate(III). *J. Am. Chem. Soc.* **1982**, *104*, 5092-5102.



FOR TABLE OF CONTENTS ONLY

TEXT FOR GRAPHICAL ABSTRACT. A new generalizable method based on integrative EPR and docking techniques was used to discriminate the strength of *non-covalent* interactions between  $V^{IV}O$  compounds and lysozyme. Several interaction sites are possible on the protein surface and the binding energy determines the distribution of the metal species between the sites and aqueous solution and the type of EPR signal (*rigid limit, slow-tumbling or isotropic*).

GRAPHICAL ABSTRACT

